Chapter 1

Introduction and Literature Survey

1. Introduction

1.1 An overview of future renewable energy demand

One of humanity's most significant challenges in the 21st century is to provide energy assurance to the ascending global population with clean and sustainable energy sources [1, 2]. To attain this challenge, the scientific and research fraternities have been active in finding and developing environmentally benign potential alternatives of energy resources to replace fossil fuels. Out of a global scenario, the energy demand will only continue to rise into the next decade, and the necessity for replacing fossil fuels with sustainable sources will become dominant. The current prediction of global energy requirement is ~18 TWy, which may reach an unprecedented ~23 TWy in 2030 and even up to ~30 TWy by 2050 with the accelerated growth of population and expanding industrialization [2]. According to the recently released statistic, ~80% of the major energy consumed was arise from conventional, fossil-fuel-based energy sources (such as coal, petroleum oil, and natural gas); however, approximately ~20% of total energy requirements are fulfilled by the renewable energy sources, like hydropower, wind, bio-power, and solar photovoltaics, provided only [3, 4]. It has been widely acknowledged that CO_2 is one of the harmful gases and is responsible for all sorts of climate changes. It was estimated by the International Energy Agency (IEA) that only in 2017, 32507 million tonnes (Mt) of carbon dioxide was released into the atmosphere, while the prediction would be a release of 35818 Mt CO_2 by 2040 and could be an alarming threat to the human civilization [5]. The adverse effect of CO_2 build-up in the atmosphere wants lowering of CO_2 emissions with an immediate effect by the early next decade to avoid potentially catastrophic consequences for life on the Earth. The straightforward solution is to shift toward environmentally benevolent energy sources and lower carbon emissions by creating carbon-neutral circular economies. Moreover, depleted fossil fuel reserves will be creating an

alarming situation of an energy crisis, which stimulate to diversify our energy sources and drive many transitions toward renewable energy sources.

In order to decrease the dependence on fossil fuels, massive efforts have been taken to harvest renewable energy such as wind, hydroelectricity, and solar. Indeed, the most attractive solution was projected as building energy security around using abundantly available energy from solar spectrum (~120,000 TW per year) reaching the Earth's surface [1, 2]. However, solar energy is an intermittent source, which is not available all the time throughout the day, particularly at night time. Similarly, storing the excessive solar energy in the form of electrical power is not at all considered as a practical solution, as batteries/capacitors, cannot store everlasting charge to supply the energy demand of our society. This concern is primarily because of the lower energy capacity of these devices in their current form, and many researchers are focused on improving their viability. Therefore, there is an urgency to develop a renewable and clean alternative that can resolve current problems and sustain for the long-term development [6].

Molecular hydrogen gas (H_2) is a vital and promising clean energy, which has attracted much attention among the various forms of the renewable energy, mainly because it has a high gravimetric energy density (142 MJ kg^{-1}), and its only combustion by-product is pollution-free water, making it an excellent energy carrier and a potential candidate for the future low-carbon energy system [7].

Presently, approximately ~96 % of the annual total production of H_2 is performed by various processes required fossil fuels, such as methane steam reforming, naphtha/oil reforming as well as coal gasification [8, 9]. Thus, current primary hydrogen production is still highly reliant on various fossil fuel resources. The H_2 production techniques based on fossil fuels cannot solve pollution and CO_2 emission problems while the various global warming issues will be unanswered. For example, in steam methane reforming process, the simultaneous

generation of hydrogen and carbon dioxide occurred at high-temperature reaction between hydrocarbon and water [8], and various greenhouse gases (e.g., CO_2) are released into the atmosphere. Thereby, such H_2 gas production processes defy our primary aim of reducing air pollution and global warming by embracing hydrogen power.

Electrochemical water splitting or water electrolysis has been considered to be an efficient, clean, and sustainable strategy for hydrogen production, since water is both the sole starting molecule and by product in the cycle. In addition, the electricity consumed by the electrolyzer can be supplied by solar, wind, and nuclear power, which can further intensify the advantages of electrocatalytic water splitting for a complete chain of the utilization of renewable energy [6].

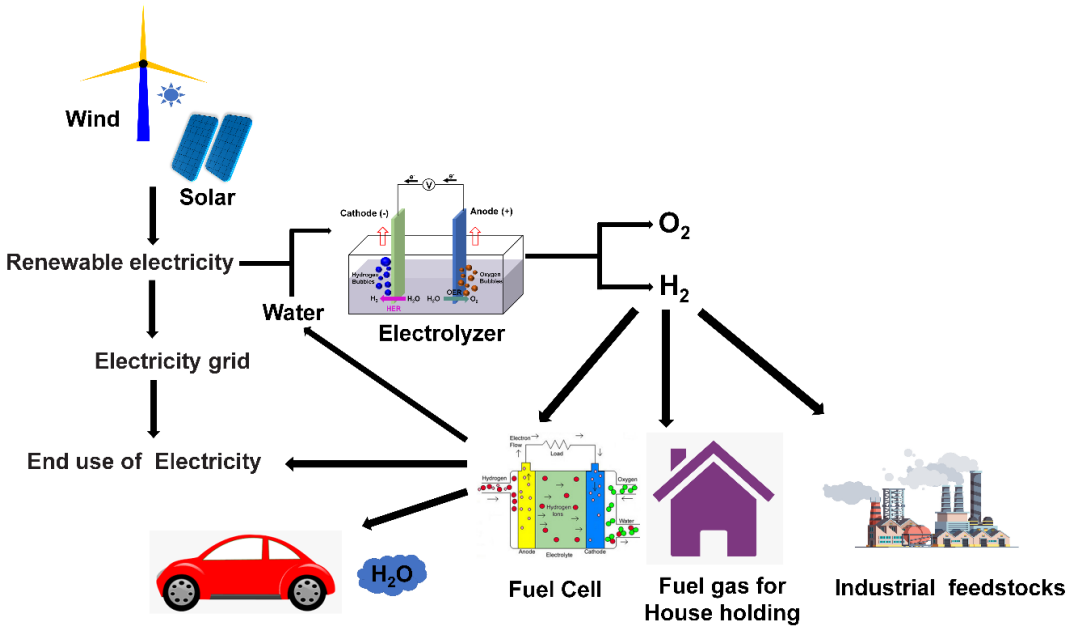

Figure 1.1: *Illustration of the hydrogen-based systems and assemblies for supplying energies in future [6].*

1.2 Electrochemistry of the hydrogen evolution reaction

Electrochemical water splitting can be divided into two half-reactions: hydrogen evolution reaction (HER) at the cathode and oxygen evolution reaction (OER) at the anode. The

hydrogen evolution catalyst (HEC) and oxygen evolution catalysts (OEC) are used as the cathode and anode, respectively, to speed the water-splitting reaction. In principle, the volume of evolved hydrogen gas should be twice as much as that of evolved oxygen gas. The device for electrochemical water splitting, i.e., an electrolyzer or electrolytic cell, is shown in Figure 1.2. Electrolyzed has three components consists of electrolyte (i.e., H_2O), a cathode, and an anode. Upon applying an external voltage to those electrodes, water molecules are dissociated into H_2 and O_2. This hydrogen yield from the water-electrolysis process can be used as fuel, while the O_2 is released into the atmosphere or can be used in any other processes.

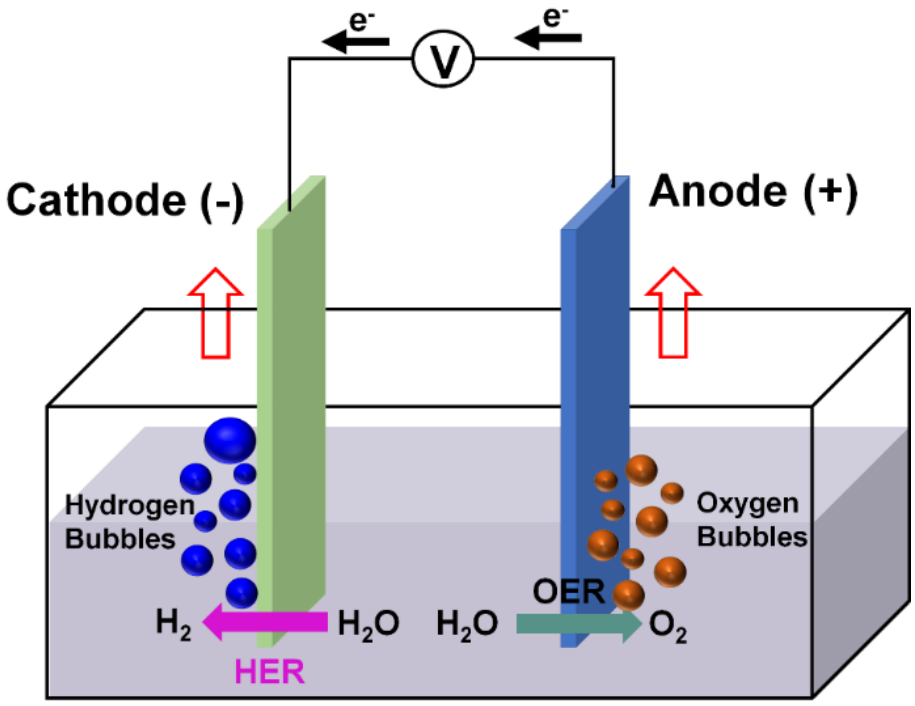

Figure 1.2: *Demonstrates a typical water electrolysis process; H_2 and O_2 are produced at the cathode and anode sides, respectively.*

According to different media (pH of the electrolyte) in which water splitting takes place, the water-splitting reaction can be expressed chemically in different ways (see below) [8].

Total reaction $H_2O \rightarrow H_2 + \frac{1}{2} O_2$ (ΔG^o = +237.2 kJ/mol, ΔE^o = 1.23 V vs. NHE) (1.1)

In acidic solution

$$\text{Cathode} \quad 2H^+ + 2e^- \rightarrow H_2 \qquad (1.2)$$

$$\text{Anode} \quad H_2O \rightarrow 2H^+ + \frac{1}{2} O_2 + 2e^- \qquad (1.3)$$

In neutral and alkaline solutions

$$\text{Cathode} \quad 2H_2O + 2e^- \rightarrow H_2 + 2OH^- \qquad (1.4)$$

$$\text{Anode} \quad 2OH^- \rightarrow H_2O + \frac{1}{2}O_2 + 2e^- \qquad (1.5)$$

1.3 Fundamentals of hydrogen evolution reaction

1.3.1 Reaction mechanism

Mechanistically, three possible principal reactions are involved during the electrochemical HER process to reduce photons in an acidic solution (Figure 1.3) or water molecules in an alkaline solution to hydrogen molecules on the surface of an electrode with a minimum external potential applied [10]. The first step is the Volmer reaction, or discharge process (Equation 1.6 and 1.7), where a proton reacts with an electron to generate an absorbed hydrogen atom (H^*) on the electrode material surface (A). These proton sources are the hydronium cations (H_3O^+) from the water molecules of acidic and alkaline electrolytes, respectively. Subsequently, the gaseous hydrogen can be generated via the Heyrovsky reaction (Equation 1.8 and 1.9) or the Tafel reaction (Equation 1.10), or both. In the Heyrovsky reaction, another proton diffuses to the absorbed hydrogen atom (H^*) and, after that, reacts with a second electron to produce H_2 (g). In the Tafel reaction, two neighboring absorbed hydrogen atoms (H^*) are combined on the electrode surface and evolve H_2 (g).

The overall HER can be written as [11]:

(1) Electrochemical hydrogen adsorption (Volmer reaction or discharge reaction)

$$H_3O^+ + A + e^- \rightarrow A - H^* + H_2O \quad \text{(Acidic medium)} \qquad (1.6)$$

$$H_2O + A + e^- \rightarrow A - H^* + OH^- \quad \text{(Alkaline medium)} \qquad (1.7)$$

(2) Electrochemical desorption (Heyrovsky reaction)

$$H^+ + e^- + A - H^* \rightarrow H_2(g)\uparrow + A \quad \text{(Acidic medium)} \qquad (1.8)$$

$$H_2O + e^- + A - H^* \rightarrow H_2(g)\uparrow + OH^- + A \quad \text{(Alkaline medium)} \qquad (1.9)$$

(3) Chemical desorption (Tafel reaction or combination reaction)

$$2A - H^* \rightarrow H_2(g)\uparrow + 2A \quad \text{(Both acidic and alkaline medium)} \qquad (1.10)$$

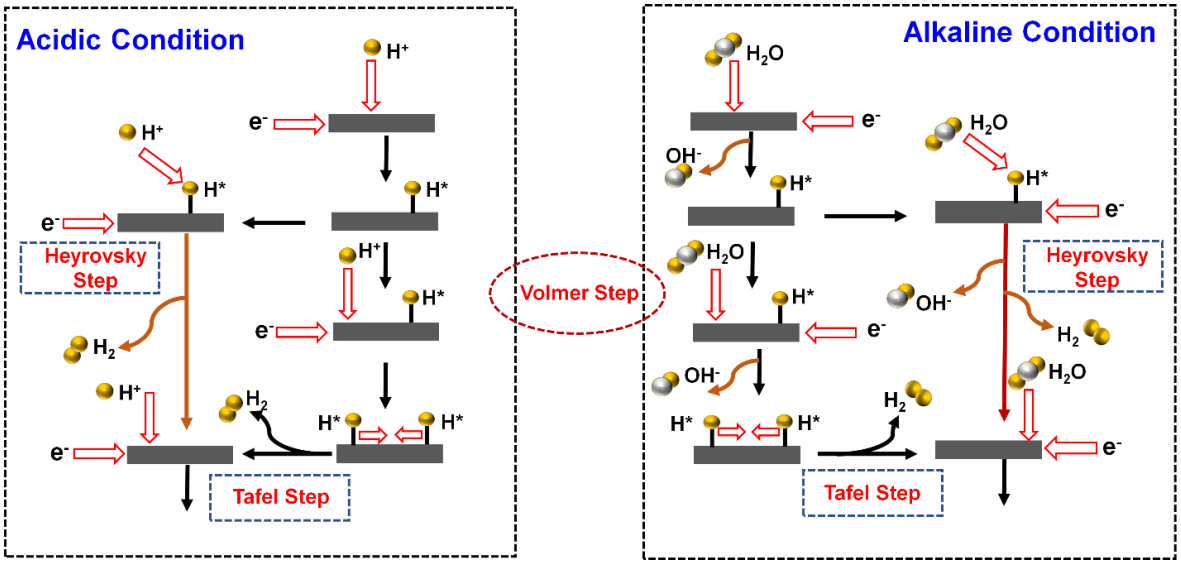

Figure 1.3: *Schematic illustration of hydrogen evaluation pathways in acidic (left) and alkaline (right) conditions [12].*

The Tafel slope (b) designates the potential difference necessary to increase or decrease the current density by 10-fold, indicating the HER mechanism process [11]. When the Volmer reaction or discharged reaction is fast and chemical desorption (combination) reaction is the rate-determining step, $b = \frac{2.3RT}{2F}$ = 29 mV/dec should be observed at 25 ºC. If the Volmer

reaction is fast and electrochemical desorptions (Heyrovsky reaction) is the rate-limiting step, $b = \frac{4.6RT}{3F}$ = 39 mV/dec should be observed at 25 ºC. If the Volmer reaction is slow $b = \frac{4.6RT}{F}$ = 116 mV/dec should be observed at 25 ºC.

1.3.2. Volcano plots

The Sabatier principle states that interaction between the reactive intermediates and catalysts should be appropriate [13]. If the interaction between the reactive intermediates and catalysts is too weak, then those intermediates will not be able to bind the surface of the catalyst, which will slow down the reaction process. On the other hand, if the interaction between the reactive intermediates and catalysts is too strong, then the reaction products will not be able to dissociate and cease the reaction by blocking the active sites of the catalyst. Measuring the ΔG_{H^*} for HER reaction processes may be used for both the H^* adsorption and H_2 desorption from a physical chemistry perspective [14]. According to the Sabatier principle, in an ideal situation, ΔG_{H^*} should be zero, and the highest HER should be j_0. Parsons established a "volcano-type" plot to relate the value of j_0 to the quantum-chemistry-based derived ΔG_{H^*} (Figure 1.4a) [15]. Recently, the "volcano-type" trend was obtained by comparing the experimental value of j_0 to the calculated value of ΔG_{H^*} using density functional theory (DFT) [16, 17]. The volcano peak is at $\Delta G_{H^*} = 0$; when $\Delta G_{H^*} < 0$, the H^* adsorption is relatively strong, causing j_0 to exponentially decrease with the decreasing value of ΔG_{H^*}. If $\Delta G_{H^*} > 0$, the H^* adsorption is relatively weak, which causes j_0 to increase exponentially as ΔG_{H^*} decreases (Figure 1.4a). Motivated by Parsons's work, Trasatti correlated the current density (log j_0) values obtained from the various metals to the calculated strength of metal-hydrogen (MH) bonds resulting in another type of "volcano" curve (Figure 1.4) [18]. With the rapid developments of computational and theoretical calculations, density functional theory (DFT) made much efforts in calculating ΔG_{H^*} values of various electrocatalysts used for water splitting reactions. This also helps in the design of volcanic curves, as demonstrated

by Norskov et al.[16] Figure 1.4b shows the volcano-plot of the relationship between the DFT-calculated ΔG_{H^*} values and the measured current density (j_0) [14, 19-23].

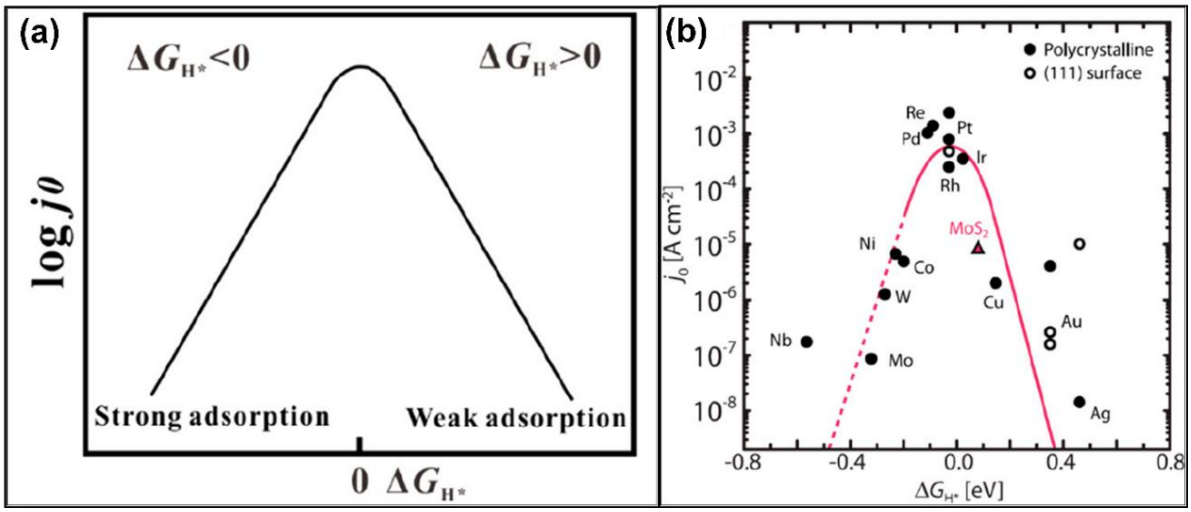

Figure 1.4: *(a) Relationship between j_0 and ΔG_{H^*} under the assumption of a Langmuir adsorption model [15]; (b) Dependence of j_0 on ΔG_{H^*} for HER on the surface of various noble metals and non-noble metals in an acidic medium [23].*

1.4. Experimental method for characterizing the electrochemical the activity of HER catalysts

Some critical parameters must be examined or computed with attention in order to determine the catalytic activity of certain HER electrocatalysts. Overpotential (η), Tafel plot, electrochemical impedance spectroscopy (EIS), stability and Cyclic Voltammetry (CV), are a few of the most important ones.

1.4.1. Overpotential (η)

Under standard conditions, the Nernst potential of HER relative to the standard hydrogen electrode (SHE) is zero according to the Nernst equation. However, experimental HER processes need a higher applied potential to overcome the kinetic barriers caused by a number of adverse factors, such as high activation energy and low energy efficiency. The catalyst's

overpotential (η) corresponds to the difference between its Nernst potential (E_{HER}) and the required potential to drive HER. Thus, the applied potential (E) was expressed as $E = E_{HER} + \eta$ [11]. Meanwhile, there will always be an inherent internal resistance (R_s) that comes from the electrocatalytic system, such as internal resistance, solvent resistance, and contact resistance of the electrochemical system, equipment, wires, etc., which causes an ohmic potential drop that needs to be fixed in current density vs. potential (j vs. E) curves as shown in Figure 1.5a [19]. Therefore, another way to represent the potential that is required to drive HER is as follows:

$E = E_{HER} + iR + \eta$; where iR is the ohmic potential drop of the current flow in the electrochemical system. In most cases, when comparing the activities of various catalysts, three distinct values correspond to current densities of 1 (η_1), 10 (η_{10}), and 100 (η_{100}) mA/cm^2 purposefully stated.

The value of η_1 is sometimes referred to as an "onset overpotential", which denotes the starting point of HER [8]. Additionally, the current density of 10 mA/cm^2 is comparable to 12.3 % of the efficiency of a solar water-splitting system, which indicates that the overpotential required for this current density might give a method for comparison [24]. Generally, η_{10} value was used to compare the activities of various catalysts in HER (Figure 1.5a), where lower η_{10} value suggests a higher catalytic activity. The loading of active material on the electrode might be different with the same geometrical area; therefore, comparing a catalytic activity at η_{10} values may not be able to tell the difference. For this reason, it is suggested to use a standard amount of catalyst (e.g., ~0.1 mg) on a glassy carbon electrode (e.g., ~0.071 cm^2) to study the HER behavior in a standard technique for future studies. Similarly, another key factor for evaluating catalysts performance for real-life applications is measuring η_{100} value at RT.

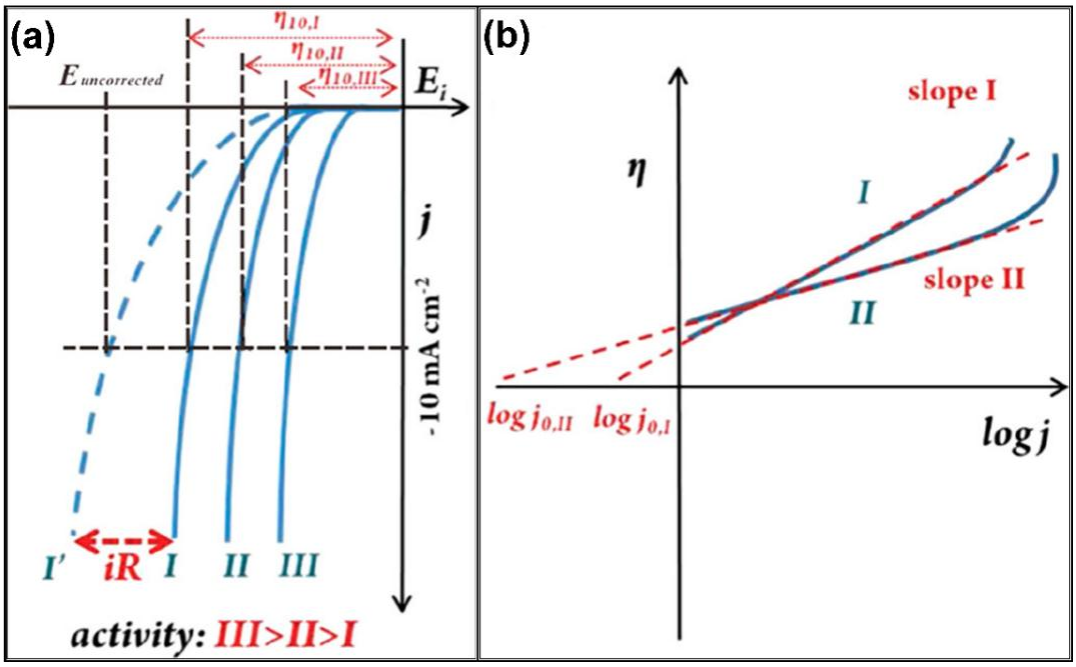

Figure 1.5: *(a) Schematic showing HER polarization curves of electrocatalysts designated with "iR" drop compensation and overpotential values; (b) schematic demonstration of Tafel plots on other electrocatalysts with the Tafel slopes and exchanges current densities indicated [19].*

1.4.2. Tafel plot

The Tafel slope (Figure 1.5b) is an intrinsic property of a catalyst that is related to the rate of HER. By plotting overpotential (η) as a function of log |j| ($\eta = b \log(\frac{j}{j_0})$, where j is the current density, j_0 is the exchange current density, and "*b*" is the Tafel slope fitted from the linear part of the Tafel plot. (Figure 1.5b). The exchange-current-density (j_0) is an important kinetic parameter showing an electrocatalyst's intrinsic catalytic activity under reversible conditions. It can be calculated by assuming η is zero. The smaller Tafel slope (b) means that a small overpotential (η) is required to deliver the same current density increment, suggesting faster electron transfer kinetics. A highly HER active electrocatalyst should have a narrow Tafel slope and high current density. Alternatively, Hu et al. recently reported a new method

to determine the Tafel slope value by plotting η vs log R_{ct}, where R_{ct} is the charge transfer resistance determined using electrochemical impedance spectroscopy (EIS) [25]. This method represents charge transfer kinetics and is ideal for nonconductive electrocatalysts.

1.4.3. Electrochemical impedance spectroscopy

As mentioned previously, the HER commonly follows Volmer (Equation 1.6 and 1.7), Heyrovsky (Equation 1.8 and 1.9), or Tafel (Equation 1.10) steps, respectively. These steps involve H^* adsorption onto the surface of the electrode. Electronic impedance spectroscopy (EIS) is used to measure the kinetics/rates assuming a Langmuir adsorption isotherm for overpotential deposited hydrogen [26, 27]. EIS Nyquist plots may also be used to determine the electrochemical measuring system's uncompensated ionic and Ohmic resistance, as well as a charge transfer resistance (R_{ct}). An R_{ct} is a term that refers to the process of charge transfer that occurs at the electrode and electrolyte interface. When it comes to HER, a lower R_{ct} value suggests a faster rate of reaction, which ultimately leads to the low overpotential. In addition, in the low-frequency region in the semicircle of the Nyquist plots, the adsorption resistance (R_{ad}) relates to the adsorption of oxidized species on the electrode surface, which indicates the onset potential of the HER. Lower the R_{ad}, the more positive the overpotential [28].

1.4.4. Stability

Stability is another important factor that must be taken into consideration when evaluating its potential for practical use. Two possible approaches are available to test the stability of an electrocatalyst: repetitive cyclic voltammetry (CV) and chronoamperometry electrolysis. The cyclic voltammetric process compares the changes in overpotential before and after a particular cycling run (e.g., 500 to 5000 runs) by conducting CV or LSV in the region, including the onset potential. A slight change of the overpotential after multiple CV indicates that the electrocatalysis is stable. In chronoamperometry, the method is to monitor the current

density variation with time at constant potential (i.e., η_{10} ~10 mA/cm^2) and the duration lasts for minimum 8-12 h. The longer duration with almost no changes or a slight change in the current density typically refers to good stability of the working electrode.

1.5. An overview of the elements used for constructing HER electrocatalysts

Figure 1.6 shows an overview of the elements that have been used for developing HER electrocatalysts. As per the known physical and chemical properties, these elements are belong to three groups: (i) noble metals platinum (Pt), ruthenium (Ru), and palladium are the state-of-the-art HER electrocatalysts; (ii) transition metals including cobalt (Co), iron (Fe), copper (Cu), nickel (Ni), copper (Cu), molybdenum (Mo), and tungsten (W); and (iii) non-metals typically used for noble metal-free HER electrocatalysts, like carbon (C), boron (B), phosphorus (P), nitrogen (N), sulfur (S), and selenium (Se). Interestingly, almost all the noble metal-free HER electrocatalysts have been demonstrated based on the above twelve non-precious elements [8].

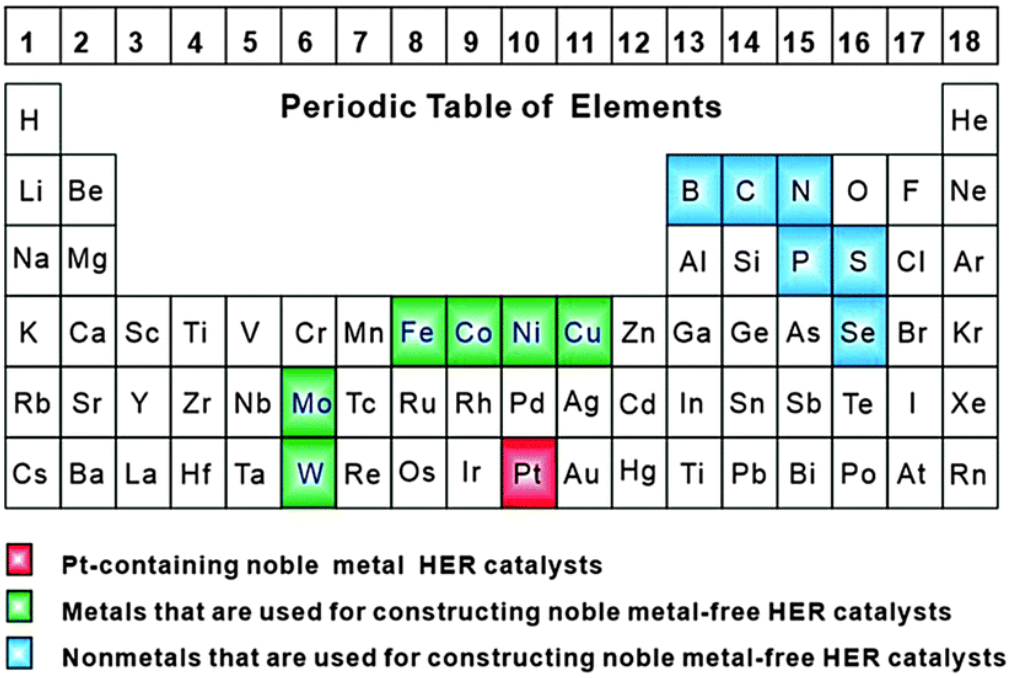

Figure 1.6: *Shows the periodic table with highlighted elements, which are used for constructing HER catalysts [8].*

Noble metal group-based catalysts (e.g., Pt, Ru, Ir, and Pd) and their derivatives have long been known as the most efficient hydrogen evaluation reaction (HER) catalysts due to their optimum Gibbs free energy for atomic hydrogen adsorption ($\Delta G_{H^*} = 0$), low activation energies for H desorption from the surface, and as well as optimal hydrogen binding energy (HBE), being capable of delivering a high exchange current density (j_0), lower Tafel slope (β) and yielding ~100% Faradaic efficiency [8, 10, 12]. However, the high cost and insufficient reserves of platinum and other noble metals restrict the broad ranges of application of platinum group metals (PGM) based catalysts for the large-scale hydrogen (H_2) production compared to the global energy demand. Therefore, reducing PGM-based noble metals loading and/or even completely replacing them with low-cost and earth-abundant non-noble metal alternatives with HER catalytic activities and durability are essential for great importance to step closer to the hydrogen economy. In recent years, research effort has been devoted to the development of state-of-the-art noble-metal electrocatalysts for electrochemical HER application, including various less-expensive and earth-abundant, noble-metal-free electrocatalysts, such as transition metals dichalcogenides (TMDs),[29-32] transition metal oxides (TMOs) [33-37], transition metal carbides (TMCs) [38-41], transition metal phosphides (TMPs) [42-45], transition metals borides (TMBs) [46-48], transition metals nitrides (TMNs),[49-53], metal alloys [54-58], and metal-free (MF) nanocomposite catalysts [59-62]. Among these transition metals dichalcogenides (TMDs) are consider as one of the highest HER active catalysts owing to their two-dimensional (2D) layered structure, exposed edge sites, high-surface-area, in-plane charge carrier mobility, catalytic activity, low-defect structure, superior mechanical and thermal properties, and chemical stability.

1.6 Two-dimensional functional nanostructures:

Since graphene invented in 2004, a rapid research interests grows among the scientists to develop two-dimensional (2D) nanostructures for functional applications, including, electronic and optoelectronic devices, energy generation and storage devices, transparent conducting oxides, sensors and biosensor, drug-delivery, and many more [63-65]. A functional nanostructure defined as a nano-scale material with multiple functionalities and those functionalities emerges from various remarkable properties of those materials, including, high electrical conductivity, good mechanical strength, good light absorption properties, and excellent electrocatalytic activity with high stability [63, 66]. However, such 2D nanomaterials and nanostructures exhibits poor charge transfer kinetics, hydrophobicity, inter-layer conductivity and, thus, are need to be re-built with various archetypes using nanoscale engineering of 0D-1D , 1D-2D, 2D-3D structures, and so on[66-68]. Specifically, in many cases, the as-synthesized 2D-layered materials required further activation to reach the desired properties of enhanced electrocatalysts [69]. Likewise, in many cases, the 2D-layered materials shows the desired mechanical stability, however, scarcity of sufficient electronic, optical, electrochemical, surface/interface properties necessary for building up functional devices [70]. Such new archetypes are not only enforce the multiple properties from all the component nanostructures in the framework, but also creates a novel nanoengineered structures with enhanced properties and electrocatalytic activity [71]. In this regard, various nanostructures have been interfaced with each other's possessing these functions, by constructing a variety of more complex hybrid structures, known as hierarchical nanostructures [71-74]. In another approach, people use various organic/inorganic functional groups to functionalized 2D-nanostructures for improving their electrocatalytic and photocatalytic properties. In particular, those functionalizations consists of many processes,

includes, doping of the 2D materials [75], attaching functional molecules with the 2D-materials surface via covalent bonding [76], and intercalations [77, 78].

1.6.1 Graphene

Graphene, a single graphitic layered sp^2 bonded 2D carbon allotropes, has created unprecedented research interests owing to its extraordinary electrical and thermal conductivity, high charge carrier density & mobility, unusual optical properties, remarkable mechanical properties and good chemical inertness [70, 79]. The fundamental building blocks of all the carbon nanostructures are a monoatomic graphitic layer that is covalently functionalized sp^2 bonded carbon atoms in a hexagonal honeycomb lattice as shown in Figure 1.7a [80]. When the single graphene layer turns into a sphere, it becomes a 0-dimensional fullerene (as shown in Figure 1.7b) and when the same layer is rolled up with respect to annoy of its axis, it forms an 1D cylindrical structure, very well known as *carbon nanotube* (Figure 1.7c). The graphene layers forms 3D bulk graphite, when the layers of single honeycomb graphitic lattices are stacked and bound by a weak van der Waals force as shown in Figure 1.7d [80]. Typically, a single monoatomic graphitic layer can be designed as monoatomic or single-layer graphene, while two and three graphitic layers are familiar as bilayer and trilayer graphene, respectively. However, more than 5-layer graphene formed a few layers of graphene and more than 10 layers graphene known as multilayer graphene or nanographite [70, 81, 82].

Graphene can be synthesized chemically via Hummers' method or modified Hummers' method, which produce graphene oxide (GO), followed by its reduction to a monoatomic layer, which exclusively known as reduced graphene oxide (rGO) [72, 83]. The as-produced single-layer rGOs are somewhat different from the graphene as the sp^2 bonded carbon atoms (C=C), which exhibits various defect centers along with covalently/non-covalently functionalized chemical species [71, 84, 85]. Such defects centers and functionalized species

also play vital role in enhancing the electrocatalytic activities of rGO compared to those graphenes produced via mechanical exfoliation and chemical vapor deposition (CVD) method.

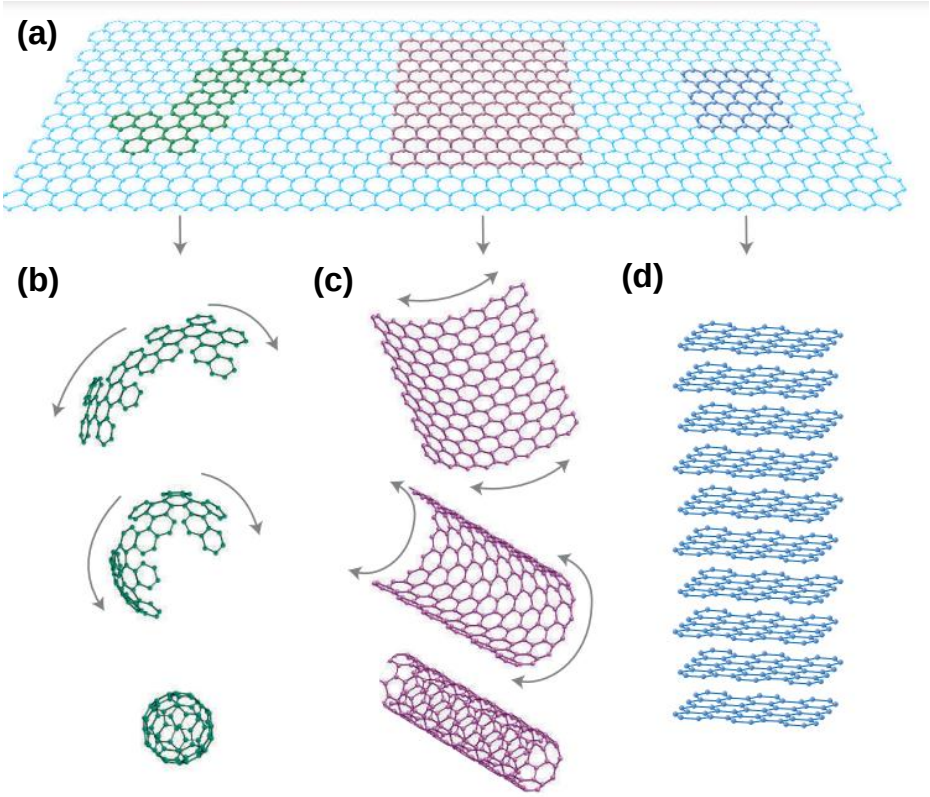

Figure 1.7: *Illustrates (a) two dimensional atomically thin single-layer graphene is the mother of all the carbon allotropes, such as, fullerene (b); carbon nanotube (c); and graphite (d) [80].*

Figure 1.8a shows a schematic depicting key properties of graphene and graphene-based materials for their applications in various energy devices, including, solar cells [86], supercapacitors [72], Li-ion batteries [87], biosensors [87], and catalysis (HER & OER) [88], as shown in Figure 1.8b. The use of rGO in electrocatalytic energy conversion reactions demonstrates immense potential in water-based-conversion reaction, like, HER, OER, and ORR using rGO as electron mediator. It is evident that ORR-related researches and

publications are almost saturated, while publications of water splitting displays tremendous research activities. Such extraordinary research-results suggest that rGO-based electrocatalysts for electrochemical energy conversion are a future emerging technology, which has versatile possibilities to develop sustainable and renewable energy innovation [89, 90].

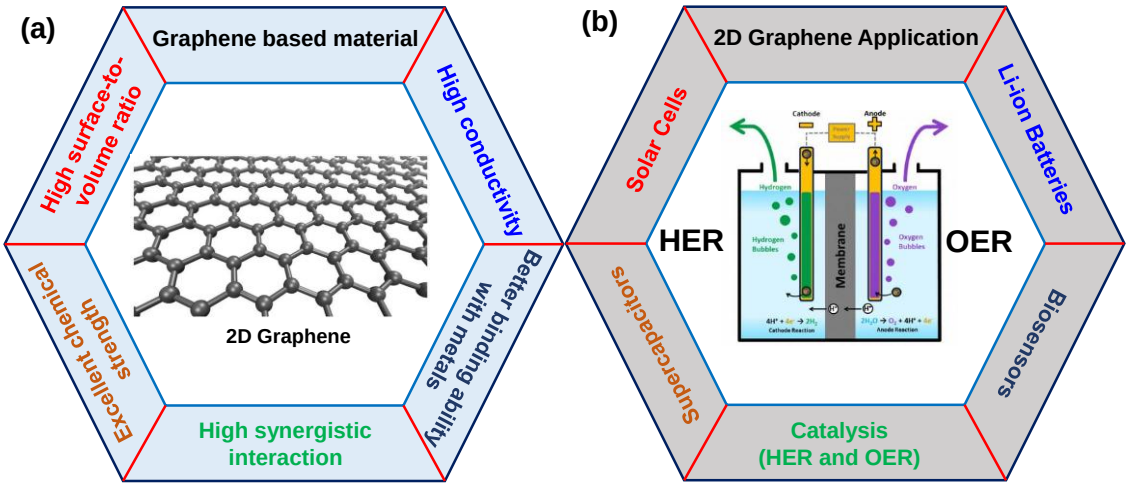

Figure 1.8: *Schematic showing (a) key properties of graphene and graphene-based materials for their applications in energy-related devices; (b) the various energy-related applications of graphene.*

1.6.2. Two-dimensional transition metal dichalcogenides (TMDs)

Two-dimensional (2D) transition metal dichalcogenides with the formula of MX_2 (M= transition metal atom; X= chalcogen atom) from more than 60 members of 2D materials (e.g., molybdenum disulfide (MoS_2), molybdenum diselenide ($MoSe_2$), tungsten disulfide (WS_2), tungsten diselenide (WSe_2), vanadium disulfide (VS_2), and vanadium diselenide (VSe_2), and so on) [29-32, 91-93]. Due to the fascinating structural and electronic properties that they possess, transition metal dichalcogenides (TMDs) are currently engaged in the electrocatalytic reactions such as oxygen evolution reaction (OER), hydrogen

evolution reaction (HER), oxygen reduction reaction (ORR), and carbon dioxide reduction reaction (CRR) [8, 94-96]. Most of the TMD-based catalysts are 2D materials; huge fundamental research confirms that the catalytically active site of TMDs is the edge site.

Among these 2D TMDs, molybdenum disulfide (MoS_2) is considered as the most promising hydrogen evaluation reaction (HER) catalyst due to its low cost, earth abundance, optimum Gibbs free energy for atomic hydrogen adsorption (ΔG_{H^*} = ~0.08 eV), bandgap turnability (1.2 eV to 1.8 eV), high surface to volume ratio, and it's two-dimensional (2D) morphology that offers a large surface area and 2D permeable channels for ion adsorption and transport [24].

1.6.2.1 Molybdenum disulfide (MoS_2)

Molybdenum disulfide (MoS_2) is one of the most popularly investigated TMDs for water electrolysis, and since last few decades, electrocatalytic activity of MoS_2 was well-acclaimed. In MoS_2, S−Mo−S layers are stacked to each layer in various ways and MoS_2 is exhibited in various polymorphs, including trigonal (1T), hexagonal (2H), and rhombohedral symmetry (3R) MoS_2 (Figure 1.9). In particular, 2H-phase of MoS_2 is composed of edge-sharing MoS_6 trigonal prisms with two layers/ unit cell, while the 3R-phase has three layers/unit cells with the same single-layer coordination as the 2H-phase [97]. On the other hand, 1T-phase of MoS_2 exhibited one layer per unit cell and molybdenum ions are coordinated in octahedral coordination. Among these three phases of MoS_2, 2H and 1T phases are widely used in HER for their unique catalytic performances.

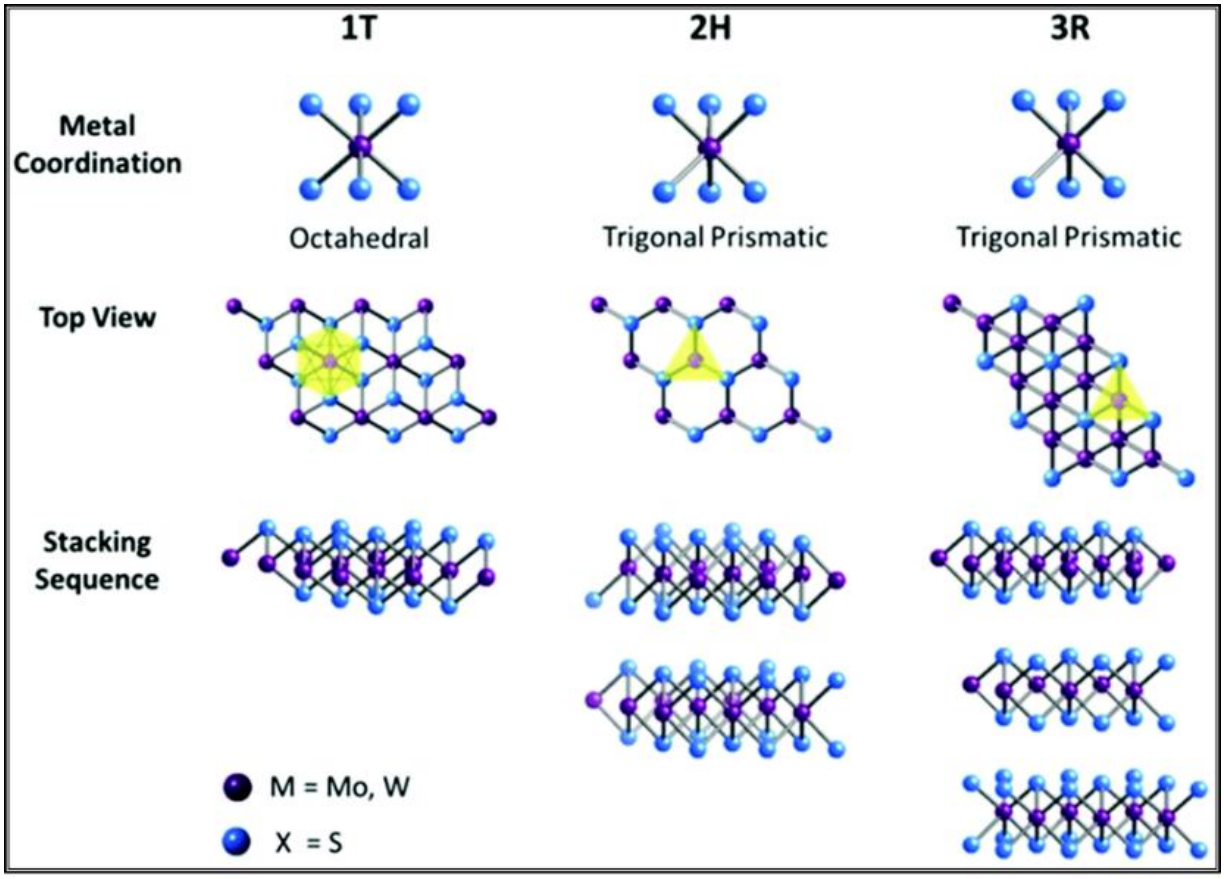

Figure 1.9: *Shows various phases of MoS_2 unit cells consist of metal coordination and stacking sequences. The way metals are put together can be octahedral or trigonal prismatic. The octahedral coordination makes it possible to stack sequences, which leads to tetragonal symmetry (1T). When trigonal prismatic single layers are stacked in different ways, they can create two different symmetries: hexagonal symmetry (2H) and rhombohedral symmetry (3R) [97].*

The study of MoS_2 on electrochemical HER may be dated back to the 1970s, and it was during this time, that researchers discovered that bulk MoS_2 crystals were non-reactive toward HER. Because of this, MoS_2 has, for a significant amount of time, been disregarded as a potentially useful HER electrocatalyst. It was reported for the first time in 2005 by Hinnemann et al. that MoS_2 was a promising HER electrocatalyst owing to its edge sites similar to that of nitrogenase, which can effectively propel HER. The computational free energy bonding (ΔG_{H*}) of Mo (1010) edge site of MoS_2 was discovered to be about 0.08 eV

at 50% hydrogen coverage by theoretical calculations (Figure 1.10a) [29]. This value is extremely near to that of Pt, which raises the possibility of MoS_2 as a promising HER electrocatalyst in theory. Soon afterward, Jaramillo et al. experimentally confirmed that the MoS_2 edges are active for HER. This study also indicated that the exchange-current-density of the materials is directly proportional to the edge length of the hexagonal particles rather than the surface area of MoS_2. It has been suggested that the catalytically active sites of MoS_2 are located at the edges of the S-Mo-S slabs, while the basal planes are thought to be catalytically inactive. The reason for the poor catalytic activity of bulk MoS_2 was found to be the low density of active edge sites (Figure 1.10b) [14].

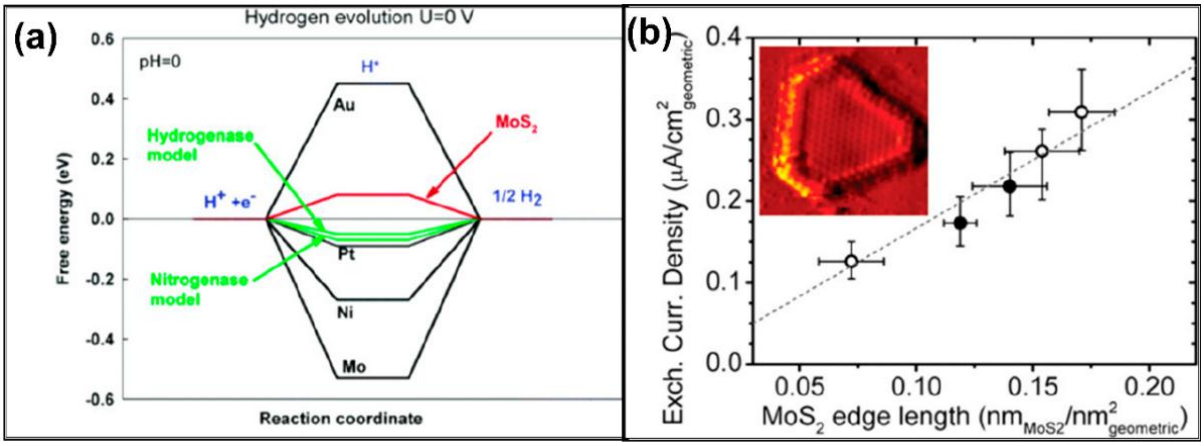

Figure 1.10: *(a) Calculated free energy diagram of HER for various electrocatalysts, including MoS_2 (0.08 eV) and different metal electrodes such as Au, Pt, Ni, and Mo at pH=0 [29]; (b) exchange current density with MoS_2 as the function of MoS_2 edge length [14].*

1.7 Strategies for improving the catalytic activity of 2H-MoS_2

Based on the active sites and semiconducting characteristics of MoS_2, research on employing MoS_2 as a HER electrocatalyst has focused on raising the edge to basal plane ratio and enhancing their activity through chemical and physical changes of the structure. Most methods include increasing the edge sites, defect engineering, heteroatom doping, phase conversion (2H to 1T), and heterostructure creation.

1.7.1 Increasing edge sites of 2H-MoS_2

Since the catalytic activity and edge-sites of MoS_2 play key role in improving HER performance, a simple strategy is to improve its specific surface area to expose more edges per unit geometric area by downsizing the structure into NPs, nanosheets, nanowires, vertical nanoflakes, mesoporous structures, etc. According to Kibsgaard et al, the active edge sites in MoS_2 films may be exposed by using double-gyroid (DG) silica as a template. The catalyst has a considerable share of active edge sites because of the bicontinuous network with nano-scale pores and a highly curved surface of MoS_2 as shown in Figure 1.11a, which described the enhancement in HER performance [98]. In addition, Wan et al. created fractal-shaped single-layer MoS_2 on a fused silica substrate and such type of MoS_2 had a considerable tensile strain and an abundance of active sites. It was confirmed that the HER catalytic activity of MoS_2 increased linearly with the number of edge sites [99]. In another method of exposing active edge sites, which was reported by Kong et al., vertically aligned molybdenum dichalcogenides ($MoSe_2$ and MoS_2) were grown on a Mo substrate to form a film surface by e-beam evaporation [100]. The comparable HER activity was tested directly with the density of the exposed edge sites (Figure 1.11b). This method of opening active edge sites have been found to be more effective than other methods reported so far. Furthermore, Yang et al. have grown parallel-stacked single-crystal 2D-MoS_2 nanobelts with the basal plane vertical to the substrate and the top surface fully covered by edge sites; these nanobelts have high electrocatalytic hydrogen evolution efficiency [101]. Also, Hu et al. demonstrated the vertical arrays of MoS_2 nanosheets, which exhibit terminated stepped surface structures produced in microwave-assisted synthesis method. The unique vertically terminated stepped surface structure with abundant exposed edge sites ensured an optimal ΔG_{H^*} (0.02 eV), which shows outstanding HER electrocatalytic performance with a low overpotential of 104 mV at 10

mA/cm^2, an exchange-current-density of 0.2 mA/cm^2, smaller Tafel slope of 121 mV/dec, and high stability in acidic medium (Figure 1.11c) [102].

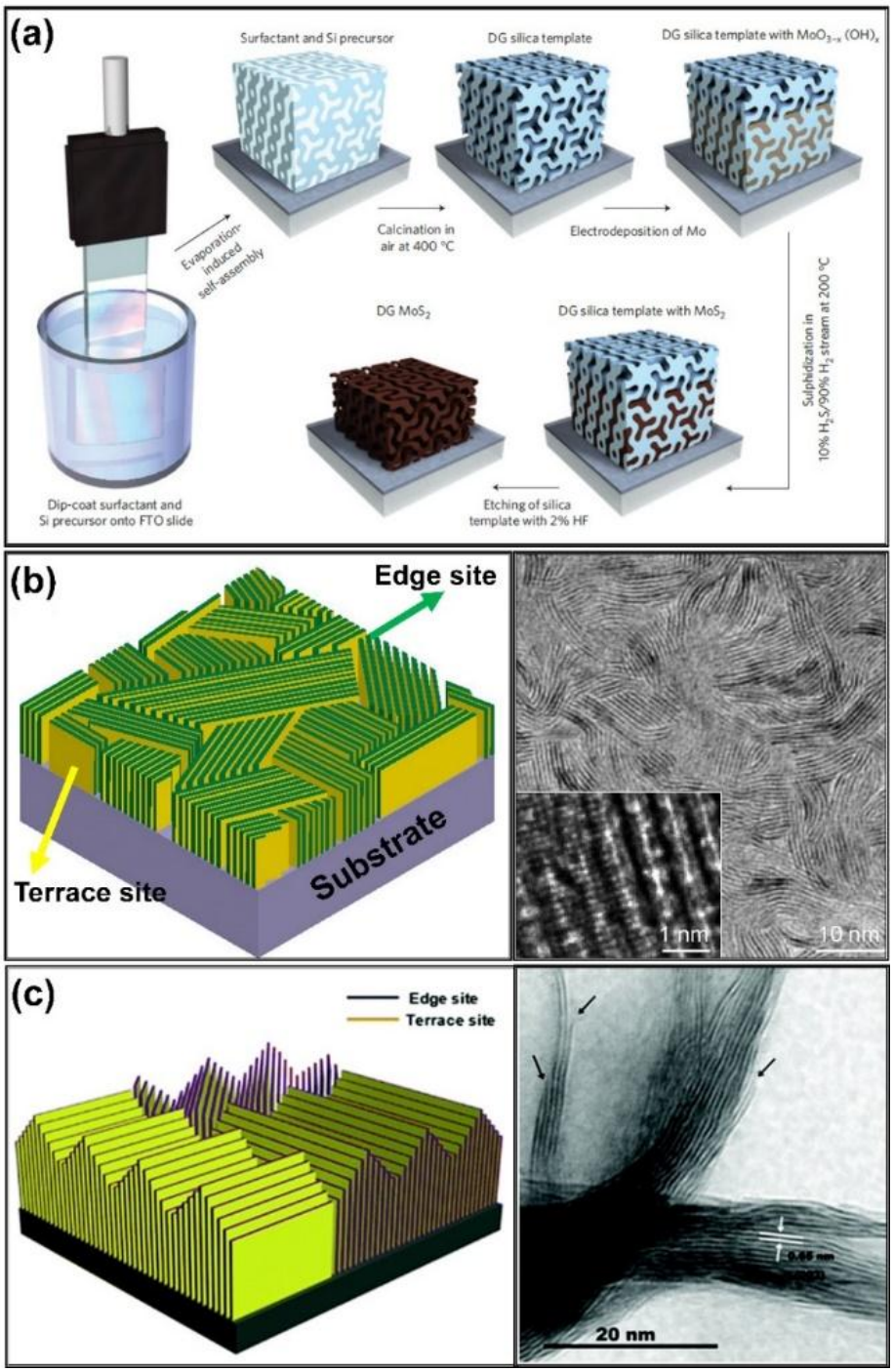

Figure 1.11: *(a) Scheme for the synthesis of mesoporous MoS_2 on double-gyroid engineering to maximally expose edge sites of MoS_2 for enhanced HER catalytic activity [98]; (b) Edge terminated MoS_2 film with maximally exposing the edges of MoS_2 layers and corresponding*

HRTEM image [100]; (c) Vertically aligned, step-edge terminated MoS_2 thin-film and corresponding TEM images [102].

1.7.2 Engineering defects in 2H-MoS_2 and the effect of strain

It is generally believed that the highly stable and semiconducting nature of the basal plane is more thermodynamically favorable than the edge sites of MoS_2. Because of such properties, the basal plane takes up a large portion of the surface sites in MoS_2 and is therefore inert toward HER in the original form of MoS_2. The unsaturated sulfur atoms at the edges are thought to be the source of the edge sites' HER catalytic activity. As a result, the edge sites may be created by introducing a structural defect in the basal plane of 2H-MoS_2. Also, it was assumed that such defects essentially modify the local density of states (DOS) and create additional energy levels between the valence (VB) and conduction bands (CB), which changes the ΔG_{H^*} to a suitable level. To activate the in-plane sites in MoS_2, there have been many different approaches, such as making sulfur vacancies and strain [103-105]. By reacting a high precursor concentration with excess thiourea, Xie et al. engineered more exposed active edge sites in MoS_2. In this case, thiourea not only acts as a reducing agent to transform Mo^{6+} to Mo^{4+}, but also as an additive to stabilize the ultra-thin structure of MoS_2. The as-synthesized defect-rich MoS_2 nanosheets displayed a high HER activity with a low onset potential of 120 mV at 10 mA/cm^2 in a 0.5 M H_2SO_4 medium, which is much lower than that of defect-free MoS_2 nanosheets as shown in Figure 1.12 a-c [106]. Motivated by this strategy, another fantastic follow-up-work was achieved by tuning the solution source in the hydrothermal process to regulate S vacancy concentrations [107-109].

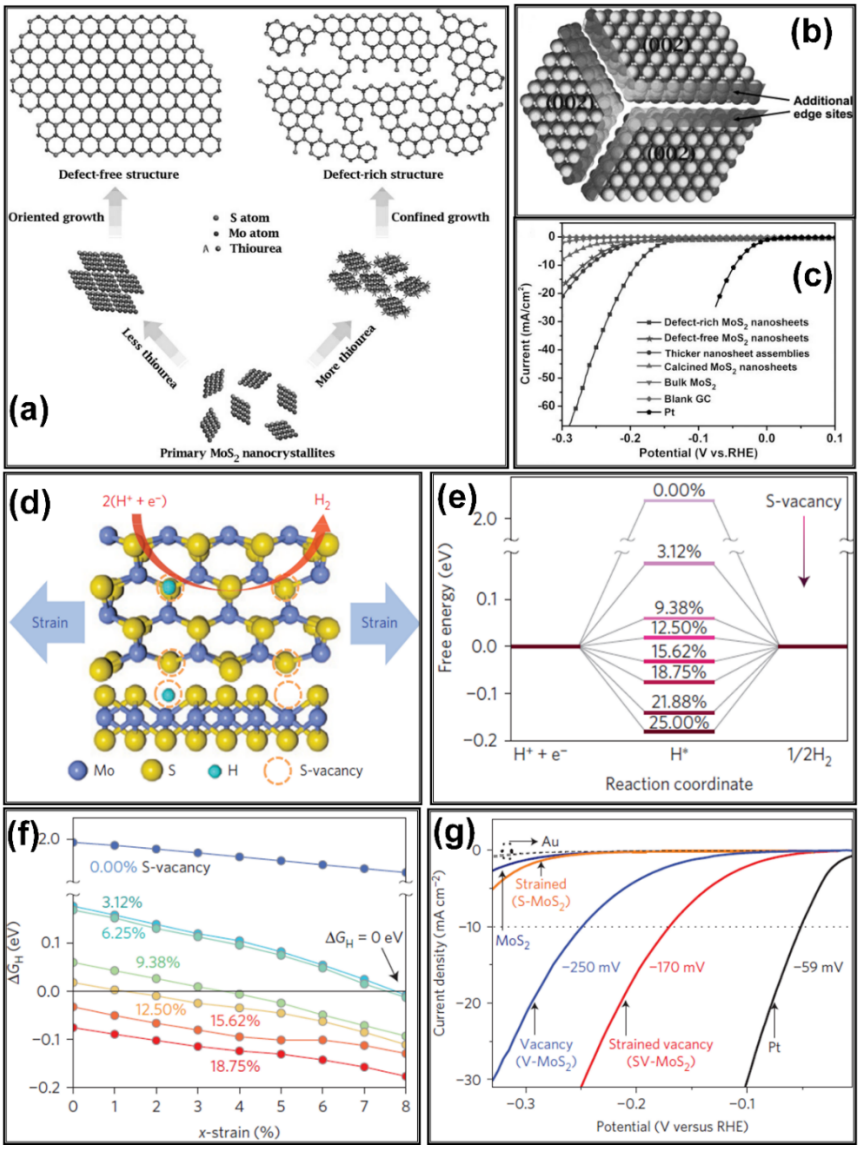

Figure 1.12: *Shows (a) schematic representation of defect-free and defect-reach MoS_2 nanosheets, (b) atomic reconcentration of defect-reach MoS_2 nanosheets with additional active sites, (c) polarization curve of different MoS_2 structures where the defect-reach MoS_2 shows the higher current density[106]; (d) schematic showing the strain-induced S-vacancies on the basal plane of 2D-MoS_2, where sulfur-vacancies act as the active sites for HER and applied strain further tunes the HER activity; (e) Free energy versus the reaction coordinate of HER for the sulfur-vacancy range from 0 to 25%; (f) ΔG_H vs. %x-strain for various S-vacancy % from 0 to 18.75%. and (g) polarization curve for the Pt electrode, Au substrate, pristine MoS_2 (S-vacancy:0% and strain: 0%) strained (S-MoS_2) MoS_2 without S-*

vacancies (S-vacancy:0% and strain: 1.5%), S-vacancy reach (V-MoS_2) MoS_2 (S-vacancy:12.5% and strain:0%) and S-vacancies with strained (SV-MoS_2) MoS_2 (S-vacancy 12.5 % and strain:1.35%) where SV-MoS_2 shows the low overpotential with enhanced HER performance [105].

In addition, the application of an Ar-plasma treatment on ultra-thin 2H-MoS_2 showed tunable-levels of 'S' vacancies and strain. Perhaps, these 'S' vacancies helps for binding hydrogen to the exposed Mo atoms, which activates the MoS_2 basal plane for HER activity. It was also found that the value of ΔG_{H^*} decreased with the percentage of sulfur vacancies and elastic strains, whereas the optimal value of ΔG_{H^*} could be achieved by tuning both of these factors simultaneously and feasibly. They also investigated the electronic structure of the defect-rich 2H-MoS_2 and showed that sulfur vacancies can contribute towards the formation of a new electronic band near the Fermi level. The position of this additional electronic-states can be shifted very closer to the Fermi level by increasing S vacancies and tensile strain as shown in Figure 1.12 d-h [105]. Kinetic studies showed that both S vacancies and out-of-plane strains could improve the catalytic activity of HER [110]. To synthesize large-scale S-vacancy-rich 2H MoS_2, an electrochemical desulfurization method can be used to reduce the inert basal plane of MoS_2. The amount of basal plane reduction can be easily changed by changing the desulfurization potential, so the HER activity of the desulfurized MoS_2 can also be tuned [111]. Li et al. recently used a sodiation/desodiation method to make 3D-ordered, unsaturated sulfur edge-enriched MoS_2 nanocrystals on carbon cloth. With a small overpotential of 136 mV at 10 mA/cm^2 in an acidic medium, this MoS_2-C hybrid electrocatalyst showed superior and more stable catalytic activity toward HER [112].

1.7.3 Constructions of heterostructures

Coupling an electrocatalyst with a conductive phase is a prominent and one of the effective methods for enhancing the overall conductivity and, subsequently, increasing the

electrocatalytic efficacy. In 2011, Li et al. demonstrated the synthesis of MoS_2 NPs decorated on rGO using Ammonium tetrathiomolybdate ($(NH_4)_2MoS_4$) and GO as a precursor. The electron conductivity of the hybrid was improved as a result of the chemical coupling of the Mo precursor with GO. This chemical coupling produced abundant open edges in the MoS_2 NPs and boosted the electron conductivity. Compared with pristine MoS_2 prepared without GO, the MoS_2 decorated rGO hybrid exhibited an extremely high HER activity and stability (Figure 1.13a) [113]. Additional theoretical studies have shown that coupled conductive materials have the potential to boost the overall HER activity of the hybrid electrocatalyst. Such chemical coupling is not only due to the improved electronic conductivity of the coupled conductive materials but also to the regulated ΔG_{H^*} value [114]. Similarly, various carbon materials, including porous carbon [112], mesoporous graphene foam [115], carbon fiber paper [116], carbon nanotube [117], and carbon cloth [118], were widely employed as a composite with MoS_2 to enhancement in HER catalysis. Apart from the carbon materials, other conductive materials, such as oxides [119], metals [120], sulfides [121], selenides [122], nitrides [123], carbides [124], and phosphide [125], were also combined with MoS_2 to enhance the overall HER catalytic activity.

The interface between MoS_2 and the other components has also been studied both theoretically and experimentally due to the development of single-phase MoS_2. The electrocatalytic activity of a MoS_2 was further modified by the van der Waals forces that are involved in the interaction with support may lead to a significant enhancement in hydrogen bonding energy, thus improving the HER catalytic activity (Figure 1.13b) as per Tsai et al. report.[126] Similarly, Li et al. reported the synthesis and characterizations of a nanohybrid composed of amorphous molybdenum sulfide (MoS_x) grafted on vertical N-doped carbon nanotube (NCNT) as an cost-effective HER catalyst (Figure 1.13c).

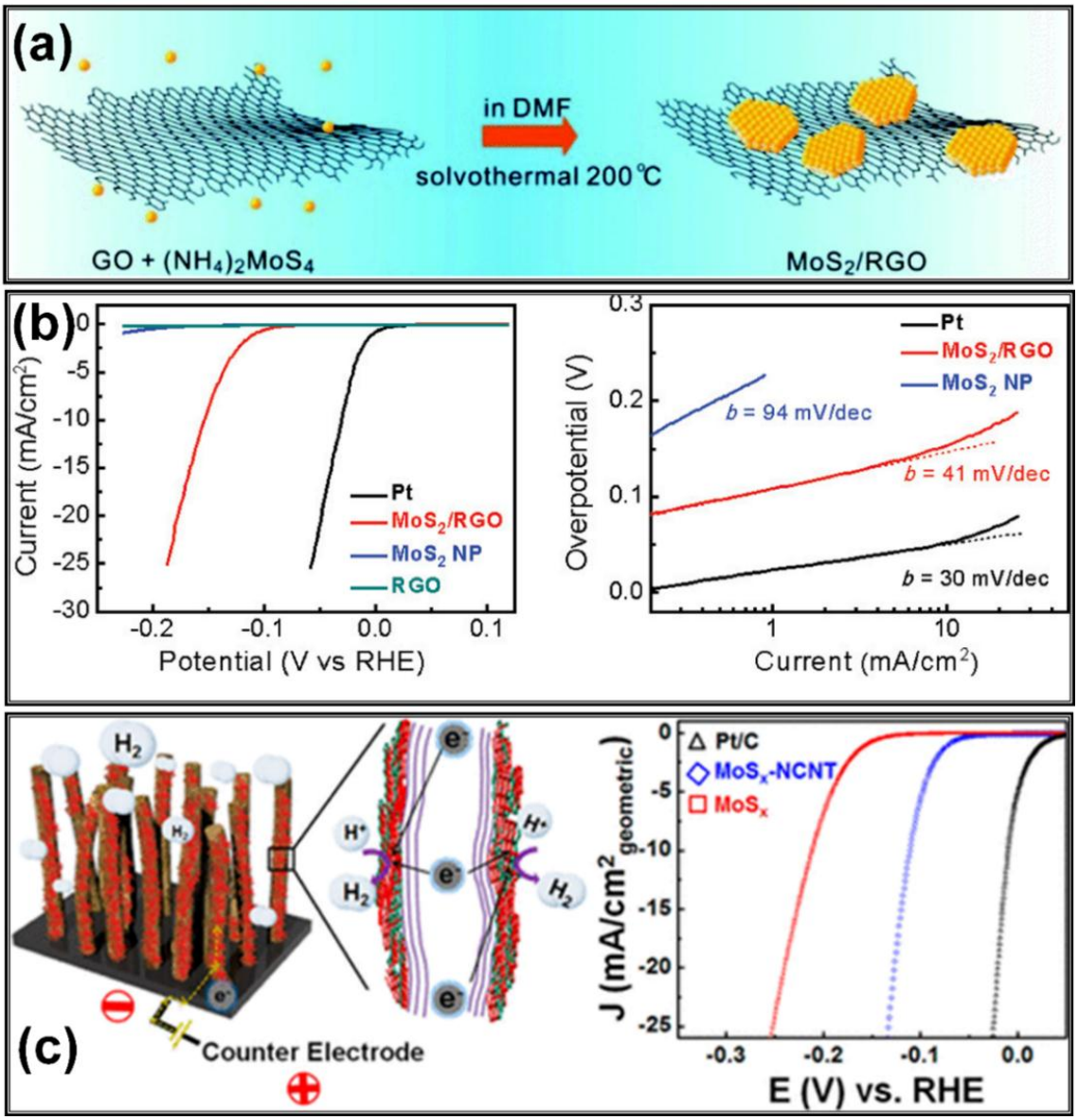

Figure 1.13: *(a) Schematic representation of the solvothermal synthesis of MoS_2/rGO hybrid; (b) polarization and Tafel curve obtained from rGO, MoS_2 NP, and MoS_2/rGO catalysts; respectively [113]; (c) HER scheme for MoS_x/NCNT forest hybrid catalyst and corresponding polarization curve [117].*

He et al. synthesized MoS_2-BP nanocomposite by depositing MoS_2 nanosheets onto the black phosphorus (BP). Because of the higher Fermi level of BP compared to that of MoS_2, electrons could transfer from BP to MoS_2. This MoS_2-BP nanocomposite resulted in escalating electron concentrations in MoS_2, which led to an increase in the intrinsic exchange

current density [127]. Luo et al. reported $Co(OH)_2$ nanoparticle intercalated MoS_2 nanosheets, in which the $Co(OH)_2$ NPs expedited water dissociation kinetics and improved the HER catalysis activity of 2D MoS_2 nanosheets [128]. Wu et al. developed MoS_2 nanosheets with $Fe_5Ni_4S_8$ at the interface on FeNi substrates. According to DFT results, such hetero-interface helps in improving the H adsorptions, which boosted the HER catalytic activity [129].

1.7.4 Heteroatom doping

Doping is an effective method used to tune the structure/electronic properties and HER activity of MoS_2. In fact, DFT calculations revealed that introducing the Co metal in the MoS_2 lattice can lower the ΔG_{H^*} of S-edges from 0.18 eV to 0.10 eV, while the Mo-edges remain the same, indicates the incorporation of Co in the MoS_2 lattice can activate the S-edges as active sites toward HER. This statement was further justified by experimental results where cobalt-doped MoS_2 showed a highly enhanced HER performance [130]. Motivated by the experimental and computational results, doping noble metals (e.g., Pt, Au, Pd, and Ru), transition metals (e.g., Co, Ni, Fe, Cu, V, and Zn), and non-metals (O, N, P, and B) into the edge or/and the basal plane assists MoS_2 for enhancing the HER performance [8, 24, 104]. Deng et al. reported the electrocatalytic activity of in-plane sulfur atoms in MoS_2 by doping single-atom platinum (Pt) into MoS_2 nanosheets (Pt-MoS_2), where Pt doping in the MoS_2 in-plane activated the sulfur atoms on the basal plane. Electrochemical results shown significant enhancement in HER performance with an ideal ΔG_{H^*} value observed after the Pt doping. These findings state that the active sites originated from the S atom rather than Pt atoms. DFT calculations also showed that the advantage of Pt doping increases the electronic states around the Femi level, resulting in a higher rate of H adsorption at in-plane S neighboring the doped Pt atoms. Similarly, in-plane doping of MoS_2 with various kinds of single metal atoms was predicted using DFT calculation as well. Dopant metal atoms like Ti, V, Mn, Fe, and Cr

were expected to bind with six S atoms, while the other group of atoms such as Ag, Pt, Co, Ni, and Pd would prefer to bind with only four S atoms, leaving the other two S atoms unsaturated. It was predicted that these two types of binding modes with a single metal atom causes the very different ΔG_{H^*} values, which promotes enhanced HER activities, as depicted in a volcano plot (Figure 1.14a) [104]. Similarly, Zhang et al. showed that adding Ni atoms to crystalline MoS_2 nanosheets was a way to accelerate the sluggish HER kinetics of MoS_2. As shown in Figure 1.14b, pristine MoS_2 shows an extraordinarily high ΔG (H_2O) (1.17 eV) and a low ΔG(OH) (5.24 eV). The $\Delta G(H_2O)$ and ΔG(OH) values were decreased to 0.66 eV and 3.46 eV, respectively, by substituting the Mo atom with the Ni atom along the edge of MoS_2. Also, the ΔG_{H^*} was changed to the desired level (-0.06 eV). These significantly decreased $\Delta G(H_2O)$, and ΔG(OH) values of Ni-doped MoS_2 nanosheets can effectively reduce the kinetic energy barrier of the initial water dissociation process and facilitate the desorption of the formed -OH from the surface of the catalysts, in addition to a suitable ΔG_{H^*} empowering Ni-doped MoS_2 with a remarkable electrochemical HER activity in alkaline solution. The DFT results suggested that Co and Fe dopants can also accelerated the HER kinetics of MoS_2 electrocatalysts [131].

Besides the metal-based dopants, non-metal (e.g., O, P, N) dopants were also used to modify the conductivity and intrinsic HER catalytic activity of MoS_2. Xie et al. group reported the synthesis of oxygen-incorporated ultrathin MoS_2 nanosheets by using a hydrothermal process at a temperature range from 140 to 200 ºC. Because of the relatively low synthesis temperature, the MoS_2 nanosheets inherited a small amount of Mo–O bonds in the molybdate precursor. It was found that the bandgap of the oxygen-incorporated MoS_2 (1.30 eV) was smaller than that of the pristine MoS_2 (1.75 eV). Oxygen incorporated MoS_2 lattice can effectively regulate the electronic structure and improve the intrinsic conductivity of pristine MoS_2 via changing the densities of states (DOS) for both valence band (VB) and conduction

band (CB), leading to the dramatically enhanced HER activity (Figure 1.14 c and Figure 1.14 d) [132].

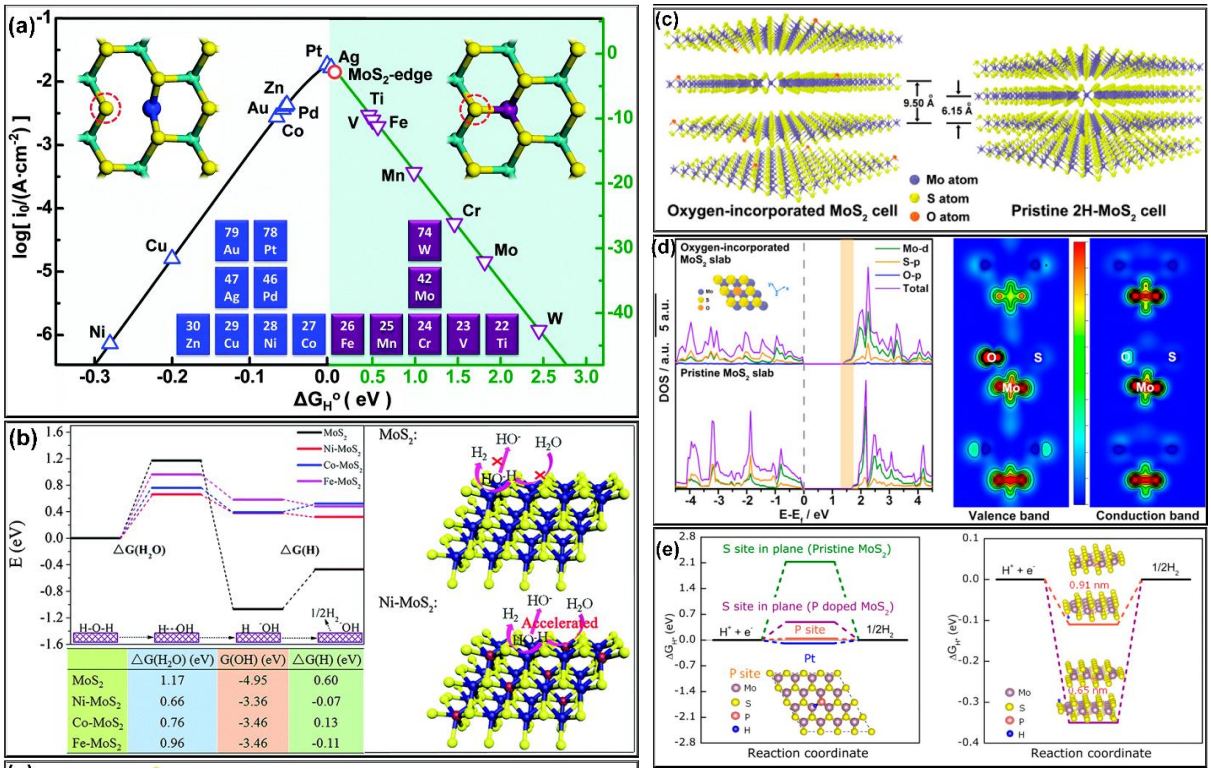

	ΔG(H2O) (eV)	G(OH) (eV)	ΔG(H) (eV)
MoS_2	1.17	-4.95	0.60
Ni-MoS_2	0.66	-3.36	-0.07
Co-MoS_2	0.76	-3.46	0.13
Fe-MoS_2	0.96	-3.46	-0.11

Figure 1.14: *(a) The relation between current (log (i_0)) vs. ΔG_H^0 presents a volcano curve, the inset graph point to a different configuration of the doped MoS_2 as coordinated with four and six S atoms. The adoption sites for H the atoms are represented by red dashed circles. The studied metal atoms are located in the periodic table, as shown by the inset at the bottom. Green, yellow, blue, and purple represent the Mo, S, and doped metal atoms [104]. (b) The results of the DFT calculation and the corresponding electrocatalytic on the surface of different catalysts under the alkaline medium. ΔG (H_2O) and ΔG (H) are related to the kinetics energy barriers for the Volume and Tafel steps on the catalysts, respectively, and ΔG (OH) is the Gibbs free energy of the adsorbed OH^- on the surface of the catalysts. In the diagram E (eV) represent the free energies of the different reactive stages. S, Mo, and Ni, are represented in yellow, blue, and red spheres [131]. (c) shows the structural modal of oxygen*

incorporated MoS_2 with large d-spacing (9.5 Å) compared to the pristine MoS_2 (6.15 Å) (d) (left) calculated DOS of the oxygen incorporated MoS_2 (top) and the pristine MoS_2 (bottom), the orange shading indicates the bandgap of pristine MoS_2 decreased after the oxygen incorporation, (right) the charge density distribution of valance band and conduction band near the oxygen atom in the oxygen incorporated MoS_2 nanosheets, respectively. Contour line of the charge density represented by black line [132]. (e) (left) HER free energy diagram for P and S site in the basal plane of pristine MoS_2 and P-doped MoS_2. Insets show that the P-doped MoS_2 with H_{ad} atom on the most active sites of the P site, (right) shows that the calculated free energy diagram for HER on P-doped MoS_2 with different interlayer spacing values measured by the experimental process (0.65 nm and 0.91 nm) [133].

In another study, Zhou et al. reported that nitrogen-doped MoS_2 nanosheets show low onset potential (156 mV vs. RHE) and smaller Tafel slope (47.5 mV/dec) than pristine MoS_2 under identical experimental conditions. This is because nitrogen doping increases the electronic conductivity of heterostructures and creates a high density of spinning electron states around the N and Mo atoms in MoS_2 nanosheets, which are the active sites for HER. Later, Liu et al. reported that the P dopant could drastically alleviate the HER catalytic activity of MoS_2 nanosheets. Experimental results show that the P-doped MoS_2 nanosheets with enlarged interlayer spacings exhibited a remarkable HER activity with an extremely low overpotential of 43 mV at 10 mA/cm^2 current density with a smaller Tafel slope of 34 mV/dec. The excellent electrocatalytic activity was due to the P dopants could act as new active sites in the basal plane with ΔG_{H^*} = 0.04 eV and significantly decreasing the ΔG_{H^*} from 2.20 eV to 0.43 eV for neighboring S atoms, as well as enhancing the intrinsic conductivity of MoS_2 nanosheets. The *p-type* dopant was also responsible for the increased interlayer distance of MoS_2, while facilitating the hydrogen adsorption and release processes (Figure 1.14e) [133].

1.7.5 Phase transformation in MoS_2

As mentioned earlier, 2H-MoS_2 possesses the semiconductor behavior, which inhibits the electron transport within it. In contrast to the 2H phase, the disordered $1T^{/}$ or 1T MoS_2 crystal structure has metallic properties and is more advantageous for electron conduction, which is improved the kinetics for HER [134-136]. The band gap of metallic 1T MoS_2 (0.006 eV) is significantly less than that of the semiconducting 2H MoS_2 (1.74 eV), as per DFT calculations [135]. Lukowski et al. reported metallic 1T MoS_2 nanosheets that were chemically exfoliated through n-butyl lithium intercalation from semiconducting 2H MoS_2 grown directly on graphite were show the remarkable improved HER catalytic activity. Structural and electrochemical analyses further confirmed that the 1T-MoS_2 polymorph shows the remarkable enhancement of intrinsic activity due to its facile electrode kinetics and low-loss electrical transport and possesses a high density of catalytically active sites as shown in Figure 1.15a and Figure 1.15 b [137].

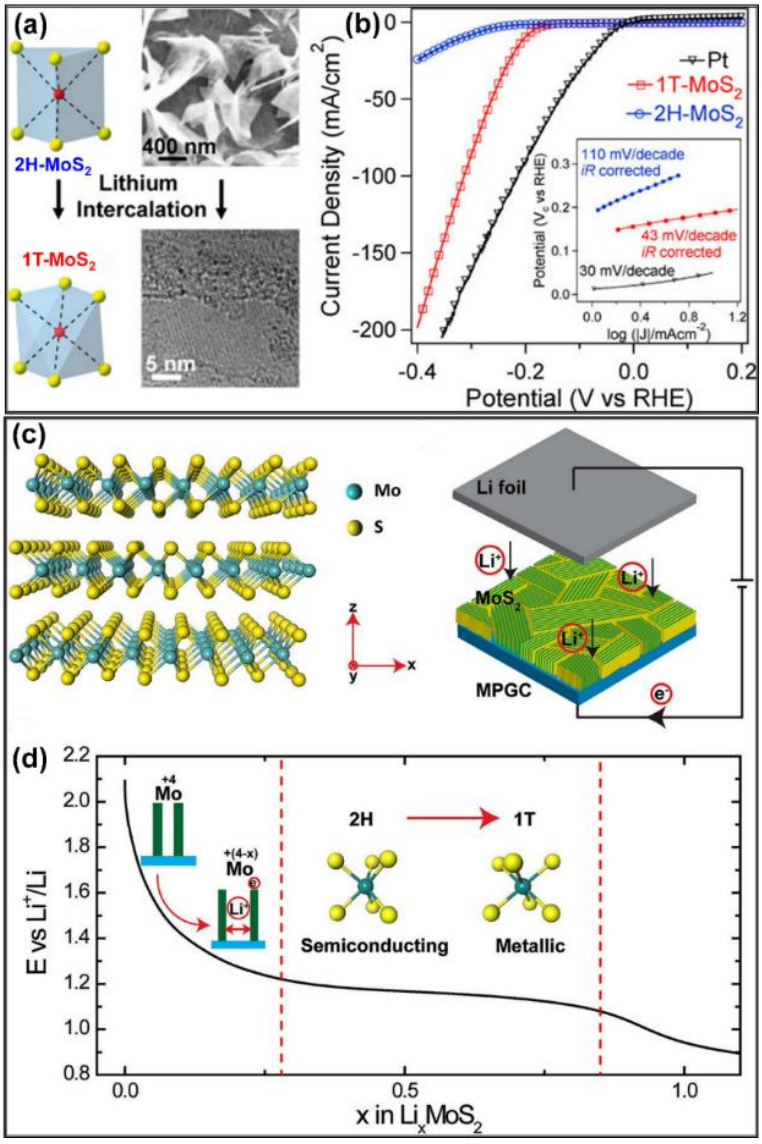

Figure 1.15: *(a) Semiconducting 2H-MoS_2 to metallic 1T-MoS_2 phase conversion by lithium intercalation and exfoliation, (b) shows the corresponding polarization curve where 1T MoS_2 exhibits the high HER catalytic activity compared to the semiconducting 2H MoS_2 [137]. (c) (right) crystal structure of 2H MoS_2, (left) Schematic of the battery testing system. The cathode is a MoS_2 nanofilm with molecular layers perpendicular to the substrate, where the yellow and green colours represent the terrace sites and edge sites, respectively. The Li foil was used as the anode. (d) The Galvanostatic discharge curve shows the lithiation process. Li intercalates into the van der Waals gaps of 2H MoS_2 to donate electrons to the slabs and expand the layer spacing of MoS_2. The voltage monotonically drops to 1.2 V*

vs. Li^+/Li to reach a Li content of 0.28 V, after which the system undergoes a semiconducting 2H MoS_2 to metallic 1T MoS_2 phase transition. The atomic structure is changed from trigonal prismatic to octahedral [139].

The theoretical analysis revealed that the HER on metallic MoS_2 followed the Volmer-Heyrovsky reaction mechanism and the Heyrovsky step is the rate-limiting step. While the Mo edges of metallic MoS_2 (1T) bear a comparable HER catalytic activity but more favorable charge transfer kinetics compared to 2H MoS_2 [138]. Likewise, Wang et al. reported the Li^+ ions intercalation in MoS_2 using the controlled potentials to transform the semiconducting 2H-MoS_2 phase to the metallic 1T-MoS_2 phase to achieve optimal electronic structures for improving the HER activity [139]. Specifically, deeper Li discharge processes leads to the increase in the interlayer spacing, which improved the HER catalytic activity (Figure 1.15c and Figure 1.15d) due to the Li-induced phase transformation in MoS_2. To synthesize 1T phase MoS_2 nanosheets, Voiry et al. employed a solvent-free intercalation process, which showed lower Tafel slopes (~40 mV/dec^1). Comparing the electrochemical performance of 1T-MoS_2 before and after oxidation, they showed that the principal active sites are not the edge sites, but the basal planes of 1T-MoS_2 were the main active sites [140].

Tang et al. performed DFT computations to understand the basal-plane activity of 1T MoS_2, and they demonstrated the affinity for binding hydrogen on the sulfur sites at the surface of 1T-MoS_2 is the essential factor for catalytic enhancement. They also reported that by replacing Mo with metal atoms such as Cu, Cr, Ni, Mn, and Cu, 1T-MoS_2 showed extraordinary HER catalytic activity than 2H-MoS_2 [138]. Attanayake et al. experimentally verified that hetero metal ions doped 1T-MoS_2, which showed the improved HER catalytic activity, confirming theoretical estimations of the previously reported data [141]. Recently, Anjum's et al. synthesized MoS_2 with a 1T-phase and numerous active sites by using the

hydrothermal and annealing process where thiourea and melamine-phosphomolybdate complex is used as a precursor showed the improved catalytic active such as overpotential (~229 mV at the current density of 10 mA/cm^2), low Tafel slope (~66 mV/dec) and high electrochemical surface area [142].

1.8 A novel hierarchical $MoNi_4/MoO_2$ nanostructures

To date, many efforts have been made to develop noble metal-free (i.e., Pt, Ru, Pd, Ir, etc) electrocatalytic electrodes and among them, transition-metal-based materials, such as MoS_2, CoP, and Ni_3N, have been extensively studied. Such MoS_2, CoP, and Ni_3N showed potential owing to their Pt-like electronic configurations with unsaturated *'d'* orbitals. Specifically, it was demonstrated that the synergistic effect of both adjacent atoms, Ni−Mo alloys hold extraordinary capabilities for hydrogen generation via water electrolysis in alkaline solutions. In this regard, Mo-Ni based alloy intermetallics (Mo_xNi_y) have been suggested as one of the promising electrocatalysts for the water electrolysis owing to their intermetallic structures, where Mo atoms exhibit superior adsorption properties towards hydrogen and Ni atoms are broadly recognized as excellent water dissociation centers [57, 143, 144]. Therefore, Ni–Mo-based alloy electrocatalysts (Mo_xNi_y) can be promising candidates to enhance the HER kinetics via water electrolysis under alkaline conditions and effectively reduce the Volmer-step energy barrier. For instance, Feng and Hu's group demonstrated the outstanding HER activity of $MoNi_4$ nanostructures supported by MoO_2 nanorods in alkaline solutions and those results justified the fair-enough prospect of Ni−Mo alloys in alkali HER, though their catalytic activity has not surpassed that of Pt till now. Zhang et al. reported $MoNi_4$ alloys covered by MoO_2 nanosheets (Figure 1.16 a-c) on Ni foam exhibiting high HER performance due to their exposed active sites, high specific surface area, and high conductivity [57]. They demonstrated the formation of $MoNi_4$ electrocatalyst in the MoO_2 cuboids (Figure 1.16 d-f) rod-like structure along with homogeneous Mo and Ni compositions (Figure 1.16 g).

Similarly, Chen et al. synthesized $MoNi_4/MoO_{3-x}$ nanorods for HER application where the dual activity of $MoNi_4$ nanocrystal embedded on MoO_{3-x} boosts the overall catalytic activity [145]. Similarly, Zhou et al. demonstrates that Mo-Ni alloy-based hollow structure (MoNi-HS) exhibits excellent HER activity in alkaline solution [146]. Lihua An et al. recently reported graphene encapsulated $MoNi_4$-$NiMoO_4$ nanorods for overall water splitting in a 1M KOH solution [88]. Similarly, Singh et al., showed that $MoNi_4/MoO_2$ nanorods can be simultaneously used as catalysts as well as the conducting channels for a TMDs-based hybrid structure [147]. We have discussed the details features of $MoNi_4/MoO_2$ nanorods and prepared such nanocomposites with entangling $MoNi_4/MoO_2$ nanostructures with graphene in chapter 3. In chapter 3, we have also demonstrated that the highly efficient $MoNi_4/MoO_2$ intermetallic nanostructures when mixed with rGO could have the potential for anticipated electrocatalytic applications in water electrolysis.

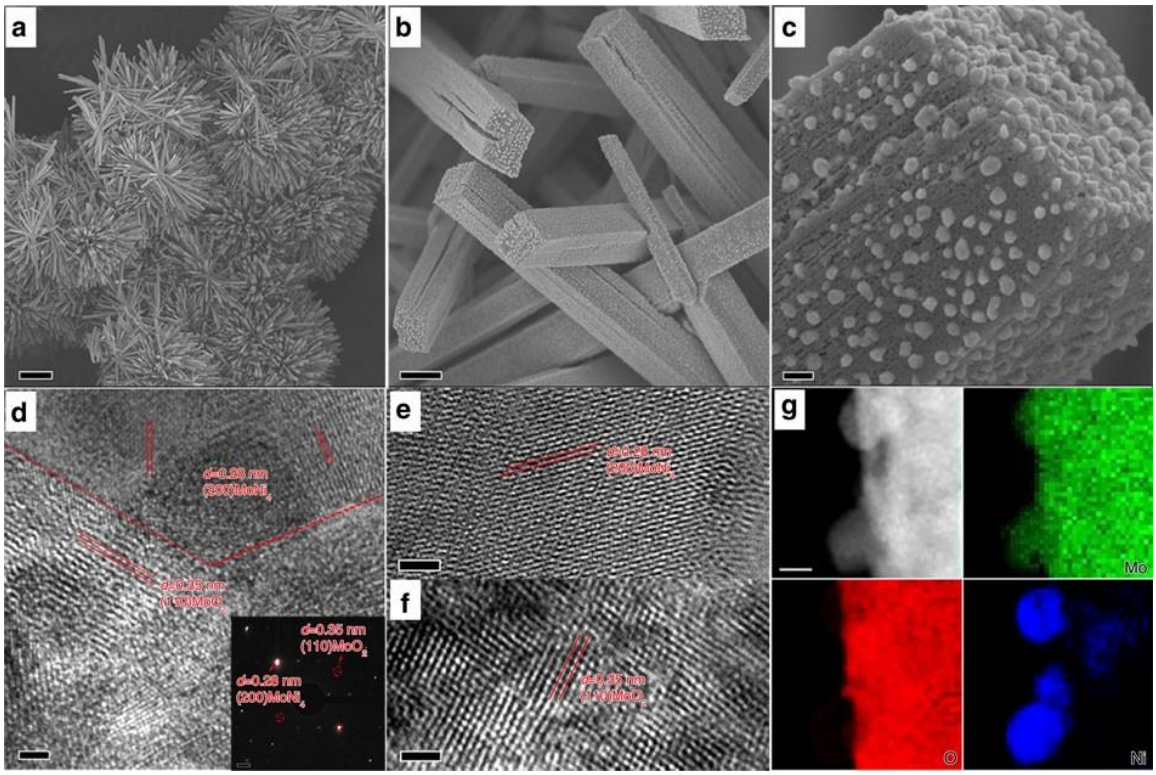

Figure 1.16: *Shows (a–c) SEM images depicting morphologies of $MoNi_4/MoO_2$@Ni; (d–f) HRTEM images of $MoNi_4/MoO_2$@Ni and the inset of (d) shows the selected area electron*

diffraction (SAED) image; (g) TEM-EDS elemental mapping images of the $MoNi_4$ electrocatalyst and the MoO_2 cuboids. [Scale bars, (a) 20 μm; (b) 1 μm; (c) 100 nm; (d–f) 2 nm; inset in d, 1 1/nm; (g) 20 nm].

1.9 Objectives of this work

In this work, we aim to develop various functional nanostructures, including 1D-2D hierarchical nanostructures, 2D-1D hybrid nanostructures and chemically functionalized nanostructures for their applications in hydrogen generation via water splitting and photocatalysis of organic pollutants. 1D-2D hierarchical nanostructures were developed by growing 1D $MoNi_4/MoO_2$ nanorod on graphene and the nanocomposites were used as electrocatalytic electrodes for hydrogen generations. We obtained that the synergistic effect of graphene's electrical conductivity and 1D $MoNi_4/MoO_2$ nanorod's electrocatalytic activity play key role in enhancing the change-transfer kinetics, thereby, improving the HER activity close to platinum. After that 2D layered MoS_2 was grown on to the 1D $MoNi_4/MoO_2$ nanorod to develop a hybrid hierarchical nanoarchitecture and the same nanostructures were applied for the water electrolysis in the alkaline medium. Interestingly, it was found that the $MoNi_4/MoO_2$ nanorods show good catalytic activity and electrical conductivity, however, they exhibited the low surface area, which play key part in the interfacial charge-transfer. Growing 2D-MoS_2 on $MoNi_4/MoO_2$ nanorod exhibited a 2D-1D nanohybrid structure with homogeneously grown forest-like vertical 2D-MoS_2 with active edge-plane like sites. This nanostructure further shows synergistic effect of faster charge-transfer kinetics (owing to 2D-MoS_2 edge-plane like structure and electrocatalytic $MoNi_4$) and good electrical conductivity and together improves the electrocatalytic properties of the nanohybrid electrode. In another approach, 2D-MoS_2 was functionalized using sulphonic acid group (-SO_3H) and we obtained that such covalent functionalizations improve localized surface electron concentrations, increase the charge transfer kinetics, and hydrophilicity. Indeed, we obtained that the SO_3H

functionalized with 2D MoS_2 basal plane as well as intercalated the few-layers MoS_2, while improving the electrocatalytically active charge transfer sites in the MoS_2. The as-synthesized SO_3H-2DMoS_2 shows many-fold enhancement in the electrocatalytic activity for water electrolysis. Finally, 2D-MoS_2 was functionalized using [SO_3H/SO_3] functional group via one pot hydrothermal synthesis process, which showed the light-induced photocatalytic properties in 2D-MoS_2. The [SO_3H/SO_3] functionalized 2D-MoS_2 showed the increase in bandgap along with expanded interlayers, which further justifies the light-induced photocatalysis of organic pollutants. To sum it all, we have developed various synergistic hierarchical nanostructures for electrocatalysis and photocatalysis, which could pave a pathway towards engineering of novel nanostructures for further use in electronics, optoelectronics, energy devices, sensors, and biosensors and so on.

References

[1] S. Chu and A. Majumdar, "Opportunities and challenges for a sustainable energy future," (in eng), *Nature,* vol. 488, no. 7411, pp. 294-303, Aug 16 2012, doi: 10.1038/nature11475.

[2] N. S. Lewis and D. G. Nocera, "Powering the planet: Chemical challenges in solar energy utilization," *Proceedings of the National Academy of Sciences,* vol. 103, no. 43, pp. 15729-15735, 2006, doi: doi:10.1073/pnas.0603395103.

[3] I. Dincer and C. Acar, "Review and evaluation of hydrogen production methods for better sustainability," *International journal of hydrogen energy,* vol. 40, no. 34, pp. 11094-11111, 2015.

[4] P. S. REN21, "Renewables 2017 global status report," *Secretariat Renewable Energy Policy Network for the,* vol. 21, 2017.

[5] I. E. Agency, "World energy outlook," ed: OECD Paris, 2018.

[6] G. Zhao, K. Rui, S. X. Dou, and W. Sun, "Heterostructures for Electrochemical Hydrogen Evolution Reaction: A Review," *Advanced Functional Materials,* vol. 28, no. 43, p. 1803291, 2018, doi: https://doi.org/10.1002/adfm.201803291.

[7] L. Schlapbach, A. Züttel, P. Gröning, O. Gröning, and P. Aebi, "Hydrogen for novel materials and devices," *Applied Physics A,* vol. 72, no. 2, pp. 245-253, 2001.

[8] X. Zou and Y. Zhang, "Noble metal-free hydrogen evolution catalysts for water splitting," *Chemical Society Reviews,* vol. 44, no. 15, pp. 5148-5180, 2015.

[9] A. Abánades, C. Rubbia, and D. Salmieri, "Thermal cracking of methane into Hydrogen for a CO_2-free utilization of natural gas," *International Journal of Hydrogen Energy,* vol. 38, no. 20, pp. 8491-8496, 2013.

[10] C. G. Morales-Guio, L.-A. Stern, and X. Hu, "Nanostructured hydrotreating catalysts for electrochemical hydrogen evolution," *Chemical Society Reviews,* vol. 43, no. 18, pp. 6555-6569, 2014, doi: 10.1039/C3CS60468C.

[11] J. Janata, "Physical Electrochemistry. Fundamentals, Techniques and Applications. By Eliezer Gileadi," *Angewandte Chemie International Edition,* vol. 50, no. 41, pp. 9538-9538, 2011, doi: https://doi.org/10.1002/anie.201104618.

[12] Z. Ge, B. Fu, J. Zhao, X. Li, B. Ma, and Y. Chen, "A review of the electrocatalysts on hydrogen evolution reaction with an emphasis on Fe, Co, and Ni-based phosphides," *Journal of Materials Science,* vol. 55, no. 29, pp. 14081-14104, 2020, doi: 10.1007/s10853-020-05010-w.

[13] S. Paul, "Hydrogenation and Dehydrogenation by Catalysis," *Berichte der Deutschen Chemischen Gesellschaft,* vol. 44, p. 17, 1911.

[14] T. F. Jaramillo, K. P. Jørgensen, J. Bonde, J. H. Nielsen, S. Horch, and I. Chorkendorff, "Identification of active edge sites for electrochemical H_2 evolution from MoS_2 nanocatalysts," *science,* vol. 317, no. 5834, pp. 100-102, 2007.

[15] R. Parsons, "The rate of electrolytic hydrogen evolution and the heat of adsorption of hydrogen," *Transactions of the Faraday Society,* vol. 54, pp. 1053-1063, 1958.

[16] J. K. Nørskov *et al.*, "Trends in the exchange current for hydrogen evolution," *Journal of The Electrochemical Society,* vol. 152, no. 3, p. J23, 2005.

[17] B. E. Conway and B. V. Tilak, "Interfacial processes involving electrocatalytic evolution and oxidation of H_2, and the role of chemisorbed H," *Electrochimica Acta,* vol. 47, no. 22, pp. 3571-3594, 2002, doi: https://doi.org/10.1016/S0013-4686(02)00329-8.

[18] S. Trasatti, "Work function, electronegativity, and electrochemical behaviour of metals: III. Electrolytic hydrogen evolution in acid solutions," *Journal of Electroanalytical Chemistry and Interfacial Electrochemistry,* vol. 39, no. 1, pp. 163-184, 1972, doi: https://doi.org/10.1016/S0022-0728(72)80485-6.

[19] Q. Gao, W. Zhang, Z. Shi, L. Yang, and Y. Tang, "Structural design and electronic modulation of transition- metal- carbide electrocatalysts toward efficient hydrogen evolution," *Advanced Materials,* vol. 31, no. 2, p. 1802880, 2019.

[20] J. Greeley, J. K. Nørskov, L. A. Kibler, A. M. El- Aziz, and D. M. Kolb, "Hydrogen evolution over bimetallic systems: Understanding the trends," *ChemPhysChem,* vol. 7, no. 5, pp. 1032-1035, 2006.

[21] Z. W. Seh, J. Kibsgaard, C. F. Dickens, I. Chorkendorff, J. K. Nørskov, and T. F. Jaramillo, "Combining theory and experiment in electrocatalysis: Insights into materials design," *Science,* vol. 355, no. 6321, p. eaad4998, 2017.

[22] V. R. Stamenkovic *et al.*, "Trends in electrocatalysis on extended and nanoscale Pt-bimetallic alloy surfaces," *Nature materials,* vol. 6, no. 3, pp. 241-247, 2007.

[23] J. Kang, J. Hwang, and B. Han, "First-principles computational screening of highly active pyrites catalysts for hydrogen evolution reaction through a universal relation

with a thermodynamic variable," *The Journal of Physical Chemistry C,* vol. 122, no. 4, pp. 2107-2112, 2018.

[24] J. Zhu, L. Hu, P. Zhao, L. Y. S. Lee, and K.-Y. Wong, "Recent Advances in Electrocatalytic Hydrogen Evolution Using Nanoparticles," *Chemical Reviews,* vol. 120, no. 2, pp. 851-918, 2020, doi: 10.1021/acs.chemrev.9b00248.

[25] H. Vrubel, T. Moehl, M. Grätzel, and X. Hu, "Revealing and accelerating slow electron transport in amorphous molybdenum sulphide particles for hydrogen evolution reaction," *Chemical Communications,* vol. 49, no. 79, pp. 8985-8987, 2013.

[26] A. Lasia, "Applications of electrochemical impedance spectroscopy to hydrogen adsorption, evolution and absorption into metals," in *Modern aspects of electrochemistry*: Springer, 2002, pp. 1-49.

[27] D. Lin and A. Lasia, "Electrochemical impedance study of the kinetics of hydrogen evolution at a rough palladium electrode in acidic solution," *Journal of Electroanalytical Chemistry,* vol. 785, pp. 190-195, 2017.

[28] J. Wang, F. Xu, H. Jin, Y. Chen, and Y. Wang, "Non- noble metal- based carbon composites in hydrogen evolution reaction: fundamentals to applications," *Advanced materials,* vol. 29, no. 14, p. 1605838, 2017.

[29] B. Hinnemann *et al.*, "Biomimetic Hydrogen Evolution: MoS_2 Nanoparticles as Catalyst for Hydrogen Evolution," *Journal of the American Chemical Society,* vol. 127, no. 15, pp. 5308-5309, 2005, doi: 10.1021/ja0504690.

[30] X. Sun *et al.*, "Semimetallic molybdenum disulfide ultrathin nanosheets as an efficient electrocatalyst for hydrogen evolution," *Nanoscale,* vol. 6, no. 14, pp. 8359-8367, 2014, doi: 10.1039/C4NR01894J.

[31] Y. Yin *et al.*, "Synergistic Phase and Disorder Engineering in 1T-$MoSe_2$ Nanosheets for Enhanced Hydrogen-Evolution Reaction," *Advanced Materials,* vol. 29, no. 28, p. 1700311, 2017, doi: https://doi.org/10.1002/adma.201700311.

[32] M. A. Lukowski *et al.*, "Highly active hydrogen evolution catalysis from metallic WS_2 nanosheets," *Energy & Environmental Science,* vol. 7, no. 8, pp. 2608-2613, 2014, doi: 10.1039/C4EE01329H.

[33] Y. Zhao *et al.*, "Defect- engineered ultrathin δ- MnO_2 nanosheet arrays as bifunctional electrodes for efficient overall water splitting," *Advanced Energy Materials,* vol. 7, no. 18, p. 1700005, 2017.

[34] X. Xie *et al.*, "P doped molybdenum dioxide on Mo foil with high electrocatalytic activity for the hydrogen evolution reaction," *Journal of Materials Chemistry A,* vol. 4, no. 5, pp. 1647-1652, 2016.

[35] J. Yan *et al.*, "Nitrogen-promoted molybdenum dioxide nanosheets for electrochemical hydrogen generation," *Journal of Materials Chemistry A,* vol. 6, no. 26, pp. 12532-12540, 2018.

[36] Z. Luo *et al.*, "Mesoporous MoO_{3-x} material as an efficient electrocatalyst for hydrogen evolution reactions," *Advanced Energy Materials,* vol. 6, no. 16, p. 1600528, 2016.

[37] R. Wu, J. Zhang, Y. Shi, D. Liu, and B. Zhang, "Metallic WO_2–carbon mesoporous nanowires as highly efficient electrocatalysts for hydrogen evolution reaction," *Journal of the American Chemical Society,* vol. 137, no. 22, pp. 6983-6986, 2015.

[38] G. Zhou *et al.*, "Coupling molybdenum carbide nanoparticles with N-doped carbon nanosheets as a high-efficiency electrocatalyst for hydrogen evolution reaction," *International Journal of Hydrogen Energy,* vol. 43, no. 19, pp. 9326-9333, 2018.

[39] Y. Zhu, G. Chen, Y. Zhong, W. Zhou, M. Liu, and Z. Shao, "An extremely active and durable Mo_2C/graphene-like carbon based electrocatalyst for hydrogen evolution reaction," *Materials today energy,* vol. 6, pp. 230-237, 2017.

[40] Z. Shi *et al.*, "Porous nanoMoC@ graphite shell derived from a MOFs-directed strategy: an efficient electrocatalyst for the hydrogen evolution reaction," *Journal of Materials Chemistry A,* vol. 4, no. 16, pp. 6006-6013, 2016.

[41] C. Lu *et al.*, "Molybdenum Carbide-Embedded Nitrogen-Doped Porous Carbon Nanosheets as Electrocatalysts for Water Splitting in Alkaline Media," *ACS Nano,* vol. 11, no. 4, pp. 3933-3942, 2017, doi: 10.1021/acsnano.7b00365.

[42] I. Paseka and J. Velicka, "Hydrogen evolution and hydrogen sorption on amorphous smooth Me-P (x)(Me= Ni, Co and Fe-Ni) electrodes," *Electrochimica Acta,* vol. 42, no. 2, pp. 237-242, 1997.

[43] P. Liu and J. A. Rodriguez, "Catalysts for hydrogen evolution from the [NiFe] hydrogenase to the Ni_2P (001) surface: the importance of ensemble effect," *Journal of the American Chemical Society,* vol. 127, no. 42, pp. 14871-14878, 2005.

[44] E. J. Popczun *et al.*, "Nanostructured nickel phosphide as an electrocatalyst for the hydrogen evolution reaction," *Journal of the American Chemical Society,* vol. 135, no. 25, pp. 9267-9270, 2013.

[45] P. Xiao *et al.*, "Molybdenum phosphide as an efficient electrocatalyst for the hydrogen evolution reaction," *Energy & Environmental Science,* vol. 7, no. 8, pp. 2624-2629, 2014.

[46] B. Albert and H. Hillebrecht, "Boron: Elementary Challenge for Experimenters and Theoreticians," *Angewandte Chemie International Edition,* vol. 48, no. 46, pp. 8640-8668, 2009, doi: https://doi.org/10.1002/anie.200903246.

[47] Y. Pan *et al.*, "Monodispersed nickel phosphide nanocrystals with different phases: synthesis, characterization and electrocatalytic properties for hydrogen evolution," *Journal of Materials Chemistry A,* vol. 3, no. 4, pp. 1656-1665, 2015, doi: 10.1039/C4TA04867A.

[48] S. Gupta, N. Patel, A. Miotello, and D. C. Kothari, "Cobalt-Boride: An efficient and robust electrocatalyst for Hydrogen Evolution Reaction," *Journal of Power Sources,* vol. 279, pp. 620-625, 2015, doi: https://doi.org/10.1016/j.jpowsour.2015.01.009.

[49] J. Miao *et al.*, "Polyoxometalate- derived hexagonal molybdenum nitrides (MXenes) supported by boron, nitrogen codoped carbon nanotubes for efficient electrochemical hydrogen evolution from seawater," *Advanced Functional Materials,* vol. 29, no. 8, p. 1805893, 2019.

[50] M.-Q. Wang *et al.*, "Engineering the nanostructure of molybdenum nitride nanodot embedded N-doped porous hollow carbon nanochains for rapid all pH hydrogen evolution," *Journal of Materials Chemistry A,* vol. 6, no. 30, pp. 14734-14741, 2018.

[51] Z. Xing, Q. Li, D. Wang, X. Yang, and X. Sun, "Self-supported nickel nitride as an efficient high-performance three-dimensional cathode for the alkaline hydrogen evolution reaction," *Electrochimica Acta,* vol. 191, pp. 841-845, 2016.

[52] Z. Xu *et al.*, "In-situ formed hydroxide accelerating water dissociation kinetics on Co3N for hydrogen production in alkaline solution," *ACS applied materials & interfaces,* vol. 10, no. 26, pp. 22102-22109, 2018.

[53] Y. Zhang, Y. Xie, Y. Zhou, X. Wang, and K. Pan, "Well dispersed Fe_2N nanoparticles on surface of nitrogen-doped reduced graphite oxide for highly efficient electrochemical hydrogen evolution," *Journal of Materials Research,* vol. 32, no. 9, pp. 1770-1776, 2017.

[54] G. Yuan *et al.*, "Aqueous substitution synthesis of platinum modified amorphous nickel hydroxide on nickel foam composite electrode for efficient and stable hydrogen evolution," *International Journal of Hydrogen Energy,* vol. 44, no. 28, pp. 14258-14265, 2019, doi: https://doi.org/10.1016/j.ijhydene.2019.03.142.

[55] J. Su, Y. Yang, G. Xia, J. Chen, P. Jiang, and Q. Chen, "Ruthenium-cobalt nanoalloys encapsulated in nitrogen-doped graphene as active electrocatalysts for producing hydrogen in alkaline media," *Nature Communications,* vol. 8, no. 1, p. 14969, 2017, doi: 10.1038/ncomms14969.

[56] I. A. Raj and K. I. Vasu, "Transition metal-based hydrogen electrodes in alkaline solution - electrocatalysis on nickel based binary alloy coatings," *Journal of Applied Electrochemistry,* vol. 20, no. 1, pp. 32-38, 1990, doi: 10.1007/BF01012468.

[57] J. Zhang *et al.*, "Efficient hydrogen production on $MoNi_4$ electrocatalysts with fast water dissociation kinetics," *Nature Communications,* vol. 8, no. 1, p. 15437, 2017, doi: 10.1038/ncomms15437.

[58] J. Deng, P. Ren, D. Deng, L. Yu, F. Yang, and X. Bao, "Highly active and durable non-precious-metal catalysts encapsulated in carbon nanotubes for hydrogen evolution reaction," *Energy & Environmental Science,* vol. 7, no. 6, pp. 1919-1923, 2014, doi: 10.1039/C4EE00370E.

[59] Y. Ito, W. Cong, T. Fujita, Z. Tang, and M. Chen, "High Catalytic Activity of Nitrogen and Sulfur Co-Doped Nanoporous Graphene in the Hydrogen Evolution Reaction," *Angewandte Chemie International Edition,* vol. 54, no. 7, pp. 2131-2136, 2015, doi: https://doi.org/10.1002/anie.201410050.

[60] T. Li *et al.*, "Functionalized Carbon Nanotubes for Highly Active and Metal-Free Electrocatalysts in Hydrogen Evolution Reaction," *Electrocatalysis,* vol. 9, no. 5, pp. 573-581, 2018, doi: 10.1007/s12678-017-0452-0.

[61] Y. Zheng *et al.*, "Toward Design of Synergistically Active Carbon-Based Catalysts for Electrocatalytic Hydrogen Evolution," *ACS Nano,* vol. 8, no. 5, pp. 5290-5296, 2014, doi: 10.1021/nn501434a.

[62] X. Yue, S. Huang, J. Cai, Y. Jin, and P. K. Shen, "Heteroatoms dual doped porous graphene nanosheets as efficient bifunctional metal-free electrocatalysts for overall water-splitting," *Journal of Materials Chemistry A,* vol. 5, no. 17, pp. 7784-7790, 2017, doi: 10.1039/C7TA01957B.

[63] K. Choudhary and F. Tavazza, "1 - Discovery and characterization of 2D materials and their heterostructures," in *2D Nanoscale Heterostructured Materials*, S. Jit and S. Das Eds.: Elsevier, 2020, pp. 1-11.

[64] U. Gupta, D. Gautam, V. Jain, and B. Mukherjee, "2 - Design and synthesis of two-dimensional materials and their heterostructures," in *2D Nanoscale Heterostructured Materials*, S. Jit and S. Das Eds.: Elsevier, 2020, pp. 13-54.

[65] C. Kumar, S. Das, and S. Jit, "7 - Device physics and device integration of two-dimensional heterostructures," in *2D Nanoscale Heterostructured Materials*, S. Jit and S. Das Eds.: Elsevier, 2020, pp. 195-214.

[66] N. Briggs *et al.*, "A roadmap for electronic grade 2D materials," *2D Materials,* vol. 6, no. 2, p. 022001, 2019/01/17 2019, doi: 10.1088/2053-1583/aaf836.

[67] S. Das *et al.*, "Synthesis and characterization of self-organized multilayered graphene-carbon nanotube hybrid films," *Journal of Materials Chemistry,* vol. 21, no. 20, 2011.

[68] S. Das *et al.*, "Synthesis of graphene-CoS electro-catalytic electrodes for dye sensitized solar cells," *Carbon,* vol. 50, no. 13, pp. 4815-4821, 2012, doi: http://dx.doi.org/10.1016/j.carbon.2012.06.006.

[69] A. Devadoss, N. Srinivasan, V. P. Devarajan, A. N. Grace, and S. Pitchaimuthu, "8 - Electrocatalytic properties of two-dimensional transition metal dichalcogenides and

their hetrostructures in energy applications," in *2D Nanoscale Heterostructured Materials*, S. Jit and S. Das Eds.: Elsevier, 2020, pp. 215-241.

[70] S. Das, M. Kim, J.-w. Lee, and W. Choi, "Synthesis, Properties, and Applications of 2-D Materials: A Comprehensive Review," *Critical Reviews in Solid State and Materials Sciences*, vol. 39, no. 4, pp. 231-252, 2014, doi: 10.1080/10408436.2013.836075.

[71] R. Bhattacharyya *et al.*, "Graphene oxide-ferrite hybrid framework as enhanced broadband absorption in gigahertz frequencies," *Scientific Reports*, vol. 9, no. 1, p. 12111, 2019, doi: 10.1038/s41598-019-48487-5.

[72] D. Biplab Kumar Kuila and Shaikh Mohammed Zaeem and Soumili Daripa and Kanak Kaushik and Saral Kumar Gupta and Santanu, "Mesoporous Mn_3O_4 coated reduced graphene oxide for high-performance supercapacitor applications," *Materials Research Express*, vol. 6, no. 1, p. 015037, 2019.

[73] P. Vabbina *et al.*, "Highly Sensitive Wide Bandwidth Photodetector Based on Internal Photoemission in CVD Grown p-Type MoS_2/Graphene Schottky Junction," *Acs Applied Materials & Interfaces*, vol. 7, no. 28, pp. 15206-15213, 2015, doi: 10.1021/acsami.5b00887.

[74] A. Devadoss *et al.*, "Synergistic Metal–Metal Oxide Nanoparticles Supported Electrocatalytic Graphene for Improved Photoelectrochemical Glucose Oxidation," *ACS Applied Materials & Interfaces*, vol. 6, no. 7, pp. 4864-4871, 2014, doi: 10.1021/am4058925.

[75] S. Das *et al.*, "Amplifying Charge-Transfer Characteristics of Graphene for Triiodide Reduction in Dye-Sensitized Solar Cells," *Advanced Functional Materials*, 10.1002/adfm.201101191, 2011.

[76] S. Das *et al.*, "Effect of HNO_3 functionalization on large scale graphene for enhanced tri-iodide reduction in dye-sensitized solar cells," *Journal of Materials Chemistry,* vol. 22, no. 38, pp. 20490-20497, 2012.

[77] E. Pollak *et al.*, "The Interaction of Li+ with Single-Layer and Few-Layer Graphene," (in English), *Nano Letters,* Article vol. 10, no. 9, pp. 3386-3388, 2010, doi: 10.1021/nl101223k.

[78] Y. Wang, D. Yan, S. El Hankari, Y. Zou, and S. Wang, "Recent Progress on Layered Double Hydroxides and Their Derivatives for Electrocatalytic Water Splitting," *Advanced Science,* vol. 5, no. 8, p. 1800064, 2018, doi: 10.1002/advs.201800064.

[79] S. Das, P. Sudhagar, Y. S. Kang, and W. Choi, "Synthesis and Characterization of Graphene," in *Carbon Nanomaterials for Advanced Energy Systems*: John Wiley & Sons, Inc, 2015, pp. 85-131.

[80] A. K. Geim and K. S. Novoselov, "The rise of graphene," *Nat Mater,* vol. 6, no. 3, pp. 183-191, 2007, 10.1038/nmat1849.

[81] S. Das and W. Choi, "Graphene Synthesis," in *Graphene: Synthesis and Applications*, vol. 3, W. Choi and J.-w. Lee Eds., 1st ed. (Nanomaterials and Their Applications, M. Meyyappan, Ed. Boca Raton: Taylor & Francis Group, 2011, ch. 2, pp. 27-63.

[82] P. S. Santanu Das, Yong Soo Kang and W. Choi, "Graphene synthesis and application for solar cells," *Journal of Materials Research,* vol. 29, no. 03, pp. 299--319, 2014 2014.

[83] O. C. Compton and S. T. Nguyen, "Graphene Oxide, Highly Reduced Graphene Oxide, and Graphene: Versatile Building Blocks for Carbon-Based Materials," *Small*, vol. 6, no. 6, pp. 711-723, 2010, doi: https://doi.org/10.1002/smll.200901934.

[84] D. R. Dreyer, S. Park, C. W. Bielawski, and R. S. Ruoff, "The chemistry of graphene oxide," (in English), *Chemical Society Reviews,* Review vol. 39, no. 1, pp. 228-240, 2010, doi: 10.1039/b917103g.

[85] R. Bhattacharyya, V. Kumar Singh, S. Bhattacharyya, P. Maiti, and S. Das, "Defect reconstructions in graphene for excellent broadband absorption properties with enhanced bandwidth," *Applied Surface Science,* vol. 537, p. 147840, 2021, doi: https://doi.org/10.1016/j.apsusc.2020.147840.

[86] S. Das, P. Sudhagar, Y. S. Kang, and W. Choi, "Graphene synthesis and application for solar cells," *Journal of Materials Research,* vol. 29, no. 03, pp. 299-319, 2014, 10.1557/jmr.2013.297.

[87] S. Das, I. Lahiri, C. Kang, and W. Choi, "Engineering carbon nanomaterials for future applications: energy and bio-sensor," pp. 80311K-80311K, 2011, doi: 10.1117/12.883743.

[88] L. An, X. Zang, L. Ma, J. Guo, Q. Liu, and X. Zhang, "Graphene layer encapsulated $MoNi_4$-$NiMoO_4$ for electrocatalytic water splitting," *Applied Surface Science,* vol. 504, p. 144390, 2020, doi: https://doi.org/10.1016/j.apsusc.2019.144390.

[89] Y. Jia *et al.*, "A Heterostructure Coupling of Exfoliated Ni–Fe Hydroxide Nanosheet and Defective Graphene as a Bifunctional Electrocatalyst for Overall Water Splitting," *Advanced Materials,* vol. 29, no. 17, p. 1700017, 2017.

[90] S. Choi, C. Kim, J. M. Suh, and H. W. Jang, "Reduced graphene oxide-based materials for electrochemical energy conversion reactions," *Carbon Energy,* vol. 1, no. 1, pp. 85-108, 2019/09/01 2019, doi: https://doi.org/10.1002/cey2.13.

[91] V. Mazánek, C. C. Mayorga-Martinez, D. Bouša, Z. Sofer, and M. Pumera, "WSe_2 nanoparticles with enhanced hydrogen evolution reaction prepared by bipolar

electrochemistry: application in competitive magneto-immunoassay," *Nanoscale*, vol. 10, no. 48, pp. 23149-23156, 2018, doi: 10.1039/C8NR04670K.

[92] J. Xu, Y. Zhu, B. Yu, C. Fang, and J. Zhang, "Metallic 1T-VS_2 nanosheets featuring V^{2+} self-doping and mesopores towards an efficient hydrogen evolution reaction," *Inorganic Chemistry Frontiers*, vol. 6, no. 12, pp. 3510-3517, 2019, doi: 10.1039/C9QI01142K.

[93] W. Zhao *et al.*, "Colloidal synthesis of VSe_2 single-layer nanosheets as novel electrocatalysts for the hydrogen evolution reaction," *Chemical Communications*, vol. 52, no. 59, pp. 9228-9231, 2016, doi: 10.1039/C6CC03854A.

[94] H. Jin *et al.*, "Emerging two-dimensional nanomaterials for electrocatalysis," *Chemical reviews*, vol. 118, no. 13, pp. 6337-6408, 2018.

[95] D. Voiry, J. Yang, and M. Chhowalla, "Recent Strategies for Improving the Catalytic Activity of 2D TMD Nanosheets Toward the Hydrogen Evolution Reaction," *Advanced Materials*, vol. 28, no. 29, pp. 6197-6206, 2016.

[96] Q. Ding, B. Song, P. Xu, and S. Jin, "Efficient Electrocatalytic and Photoelectrochemical Hydrogen Generation Using MoS_2 and Related Compounds," *Chem*, vol. 1, no. 5, pp. 699-726, 2016.

[97] R. J. Toh, Z. Sofer, J. Luxa, D. Sedmidubský, and M. Pumera, "3R phase of MoS_2 and WS_2 outperforms the corresponding 2H phase for hydrogen evolution," *Chemical Communications*, vol. 53, no. 21, pp. 3054-3057, 2017, doi: 10.1039/C6CC09952A.

[98] J. Kibsgaard, Z. Chen, B. N. Reinecke, and T. F. Jaramillo, "Engineering the surface structure of MoS_2 to preferentially expose active edge sites for electrocatalysis," *Nature Materials*, vol. 11, no. 11, pp. 963-969, 2012, doi: 10.1038/nmat3439.

[99] Y. Wan *et al.*, "Engineering active edge sites of fractal-shaped single-layer MoS_2 catalysts for high-efficiency hydrogen evolution," *Nano Energy,* vol. 51, pp. 786-792, 2018, doi: https://doi.org/10.1016/j.nanoen.2018.02.027.

[100] D. Kong *et al.*, "Synthesis of MoS_2 and $MoSe_2$ Films with Vertically Aligned Layers," *Nano Letters,* vol. 13, no. 3, pp. 1341-1347, 2013, doi: 10.1021/nl400258t.

[101] L. Yang *et al.*, "Single-Crystal Atomic-Layered Molybdenum Disulfide Nanobelts with High Surface Activity," *ACS Nano,* vol. 9, no. 6, pp. 6478-6483, 2015, doi: 10.1021/acsnano.5b02188.

[102] J. Hu *et al.*, "Engineering stepped edge surface structures of MoS_2 sheet stacks to accelerate the hydrogen evolution reaction," *Energy & Environmental Science,* vol. 10, no. 2, pp. 593-603, 2017, doi: 10.1039/C6EE03629E.

[103] Y. Tan *et al.*, "Monolayer MoS_2 Films Supported by 3D Nanoporous Metals for High-Efficiency Electrocatalytic Hydrogen Production," *Advanced Materials,* vol. 26, no. 47, pp. 8023-8028, 2014, doi: https://doi.org/10.1002/adma.201403808.

[104] J. Deng *et al.*, "Triggering the electrocatalytic hydrogen evolution activity of the inert two-dimensional MoS_2 surface via single-atom metal doping," *Energy & Environmental Science,* vol. 8, no. 5, pp. 1594-1601, 2015, doi: 10.1039/C5EE00751H.

[105] H. Li *et al.*, "Activating and optimizing MoS_2 basal planes for hydrogen evolution through the formation of strained sulphur vacancies," *Nature Materials,* vol. 15, no. 1, pp. 48-53, 2016, doi: 10.1038/nmat4465.

[106] J. Xie *et al.*, "Defect-Rich MoS_2 Ultrathin Nanosheets with Additional Active Edge Sites for Enhanced Electrocatalytic Hydrogen Evolution," *Advanced Materials,* vol. 25, no. 40, pp. 5807-5813, 2013, doi: https://doi.org/10.1002/adma.201302685.

[107] Y. Guo, X. Zhang, X. Zhang, and T. You, "Defect- and S-rich ultrathin MoS_2 nanosheet embedded N-doped carbon nanofibers for efficient hydrogen evolution," *Journal of Materials Chemistry A,* vol. 3, no. 31, pp. 15927-15934, 2015.

[108] Y. Xu *et al.,* "Monolayer MoS_2 with S vacancies from interlayer spacing expanded counterparts for highly efficient electrochemical hydrogen production," *Journal of Materials Chemistry A,* vol. 4, no. 42, pp. 16524-16530, 2016.

[109] J. Zhang *et al.,* "Water-Soluble Defect-Rich MoS_2 Ultrathin Nanosheets for Enhanced Hydrogen Evolution," *The Journal of Physical Chemistry Letters,* vol. 10, no. 12, pp. 3282-3289, 2019, doi: 10.1021/acs.jpclett.9b01121.

[110] H. Li *et al.,* "Kinetic Study of Hydrogen Evolution Reaction over Strained MoS_2 with Sulfur Vacancies Using Scanning Electrochemical Microscopy," *Journal of the American Chemical Society,* vol. 138, no. 15, pp. 5123-5129, 2016.

[111] C. Tsai *et al.,* "Electrochemical generation of sulfur vacancies in the basal plane of MoS_2 for hydrogen evolution," *Nature Communications,* vol. 8, no. 1, p. 15113, 2017.

[112] Q. Xu, Y. Liu, H. Jiang, Y. Hu, H. Liu, and C. Li, "Unsaturated Sulfur Edge Engineering of Strongly Coupled MoS_2 Nanosheet–Carbon Macroporous Hybrid Catalyst for Enhanced Hydrogen Generation," *Advanced Energy Materials,* vol. 9, no. 2, p. 1802553, 2019, doi: https://doi.org/10.1002/aenm.201802553.

[113] Y. Li, H. Wang, L. Xie, Y. Liang, G. Hong, and H. Dai, "MoS_2 Nanoparticles Grown on Graphene: An Advanced Catalyst for the Hydrogen Evolution Reaction," *Journal of the American Chemical Society,* vol. 133, no. 19, pp. 7296-7299, 2011, doi: 10.1021/ja201269b.

[114] W. Chen, E. J. G. Santos, W. Zhu, E. Kaxiras, and Z. Zhang, "Tuning the Electronic and Chemical Properties of Monolayer MoS_2 Adsorbed on Transition Metal Substrates," *Nano Letters,* vol. 13, no. 2, pp. 509-514, 2013, doi: 10.1021/nl303909f.

[115] S.-K. Park, D. Y. Chung, D. Ko, Y.-E. Sung, and Y. Piao, "Three-dimensional carbon foam/N-doped graphene@MoS_2 hybrid nanostructures as effective electrocatalysts for the hydrogen evolution reaction," *Journal of Materials Chemistry A*, vol. 4, no. 33, pp. 12720-12725, 2016, doi: 10.103
9/C6TA03458F.

[116] Y. Yan, B. Xia, N. Li, Z. Xu, A. Fisher, and X. Wang, "Vertically oriented MoS_2 and WS_2 nanosheets directly grown on carbon cloth as efficient and stable 3-dimensional hydrogen-evolving cathodes," *Journal of Materials Chemistry A*, vol. 3, no. 1, pp. 131-135, 2015, doi: 10.1039/C4TA04858J.

[117] D. J. Li *et al.*, "Molybdenum Sulfide/N-Doped CNT Forest Hybrid Catalysts for High-Performance Hydrogen Evolution Reaction," *Nano Letters*, vol. 14, no. 3, pp. 1228-1233, 2014, doi: 10.1021/nl404108a.

[118] N. Zhang, S. Gan, T. Wu, W. Ma, D. Han, and L. Niu, "Growth Control of MoS_2 Nanosheets on Carbon Cloth for Maximum Active Edges Exposed: An Excellent Hydrogen Evolution 3D Cathode," *ACS Applied Materials & Interfaces*, vol. 7, no. 22, pp. 12193-12202, 2015, doi: 10.1021/acsami.5b02586.

[119] Z. Chen, D. Cummins, B. N. Reinecke, E. Clark, M. K. Sunkara, and T. F. Jaramillo, "Core–shell MoO_3–MoS_2 Nanowires for Hydrogen Evolution: A Functional Design for Electrocatalytic Materials," *Nano Letters*, vol. 11, no. 10, pp. 4168-4175, 2011, doi: 10.1021/nl2020476.

[120] Z. Chen *et al.*, "Interface confined hydrogen evolution reaction in zero valent metal nanoparticles-intercalated molybdenum disulfide," *Nature Communications*, vol. 8, no. 1, p. 14548, 2017/02/23 2017, doi: 10.1038/ncomms14548.

[121] J. Zhang *et al.*, "Interface Engineering of MoS_2/Ni_3S_2 Heterostructures for Highly Enhanced Electrochemical Overall-Water-Splitting Activity," *Angewandte Chemie*

International Edition, vol. 55, no. 23, pp. 6702-6707, 2016, doi: https://doi.org/10.1002/anie.201602237.

[122] M.-R. Gao *et al.*, "An efficient molybdenum disulfide/cobalt diselenide hybrid catalyst for electrochemical hydrogen generation," *Nature Communications,* vol. 6, no. 1, p. 5982, 2015, doi: 10.1038/ncomms6982.

[123] I. S. Amiinu *et al.*, "Multifunctional Mo–N/C@MoS_2 Electrocatalysts for HER, OER, ORR, and Zn–Air Batteries," *Advanced Functional Materials,* vol. 27, no. 44, p. 1702300, 2017, doi: https://doi.org/10.1002/adfm.201702300.

[124] Z. Zhao *et al.*, "Vertically Aligned MoS_2/Mo_2C hybrid Nanosheets Grown on Carbon Paper for Efficient Electrocatalytic Hydrogen Evolution," *ACS Catalysis,* vol. 7, no. 10, pp. 7312-7318, 2017, doi: 10.1021/acscatal.7b02885.

[125] M. Kim, M. A. R. Anjum, M. Lee, B. J. Lee, and J. S. Lee, "Activating MoS_2 Basal Plane with Ni_2P Nanoparticles for Pt-Like Hydrogen Evolution Reaction in Acidic Media," *Advanced Functional Materials,* vol. 29, no. 10, p. 1809151, 2019, doi: https://doi.org/10.1002/adfm.201809151.

[126] C. Tsai, F. Abild-Pedersen, and J. K. Nørskov, "Tuning the MoS_2 Edge-Site Activity for Hydrogen Evolution via Support Interactions," *Nano Letters,* vol. 14, no. 3, pp. 1381-1387, 2014, doi: 10.1021/nl404444k.

[127] R. He *et al.*, "Molybdenum Disulfide–Black Phosphorus Hybrid Nanosheets as a Superior Catalyst for Electrochemical Hydrogen Evolution," *Nano Letters,* vol. 17, no. 7, pp. 4311-4316, 2017, doi: 10.1021/acs.nanolett.7b01334.

[128] Y. Luo *et al.*, "Two-Dimensional MoS_2 Confined $Co(OH)_2$ Electrocatalysts for Hydrogen Evolution in Alkaline Electrolytes," *ACS Nano,* vol. 12, no. 5, pp. 4565-4573, 2018, doi: 10.1021/acsnano.8b00942.

[129] Y. Wu *et al.*, "Coupling Interface Constructions of $MoS_2/Fe_5Ni_4S_8$ Heterostructures for Efficient Electrochemical Water Splitting," *Advanced Materials,* vol. 30, no. 38, p. 1803151, 2018, doi: https://doi.org/10.1002/adma.201803151.

[130] J. Bonde, P. G. Moses, T. F. Jaramillo, J. K. Nørskov, and I. Chorkendorff, "Hydrogen evolution on nano-particulate transition metal sulfides," *Faraday Discussions,* vol. 140, no. 0, pp. 219-231, 2009, doi: 10.1039/B803857K.

[131] J. Zhang *et al.*, "Engineering water dissociation sites in MoS_2 nanosheets for accelerated electrocatalytic hydrogen production," *Energy & Environmental Science,* vol. 9, no. 9, pp. 2789-2793, 2016, doi: 10.1039/C6EE01786J.

[132] J. Xie *et al.*, "Controllable Disorder Engineering in Oxygen-Incorporated MoS_2 Ultrathin Nanosheets for Efficient Hydrogen Evolution," *Journal of the American Chemical Society,* vol. 135, no. 47, pp. 17881-17888, 2013, doi: 10.1021/ja408329q.

[133] P. Liu *et al.*, "P Dopants Triggered New Basal Plane Active Sites and Enlarged Interlayer Spacing in MoS_2 Nanosheets toward Electrocatalytic Hydrogen Evolution," *ACS Energy Letters,* vol. 2, no. 4, pp. 745-752, 2017.

[134] Y.-C. Lin, D. O. Dumcenco, Y.-S. Huang, and K. Suenaga, "Atomic mechanism of the semiconducting-to-metallic phase transition in single-layered MoS_2," *Nature Nanotechnology,* vol. 9, no. 5, pp. 391-396, 2014, doi: 10.1038/nnano.2014.64.

[135] G. Gao, Y. Jiao, F. Ma, Y. Jiao, E. Waclawik, and A. Du, "Charge Mediated Semiconducting-to-Metallic Phase Transition in Molybdenum Disulfide Monolayer and Hydrogen Evolution Reaction in New 1T′ Phase," *The Journal of Physical Chemistry C,* vol. 119, no. 23, pp. 13124-13128, 2015, doi: 10.1021/acs.jpcc.5b04658.

[136] X. Gan *et al.*, "2H/1T Phase Transition of Multilayer MoS_2 by Electrochemical Incorporation of S Vacancies," *ACS Applied Energy Materials,* vol. 1, no. 9, pp. 4754-4765, 2018, doi: 10.1021/acsaem.8b00875.

[137] M. A. Lukowski, A. S. Daniel, F. Meng, A. Forticaux, L. Li, and S. Jin, "Enhanced Hydrogen Evolution Catalysis from Chemically Exfoliated Metallic MoS_2 Nanosheets," *Journal of the American Chemical Society,* vol. 135, no. 28, pp. 10274-10277, 2013, doi: 10.1021/ja404523s.

[138] Q. Tang and D.-e. Jiang, "Mechanism of Hydrogen Evolution Reaction on 1T-MoS_2 from First Principles," *ACS Catalysis,* vol. 6, no. 8, pp. 4953-4961, 2016/08/05 2016.

[139] H. Wang *et al.*, "Electrochemical tuning of vertically aligned MoS_2 nanofilms and its application in improving hydrogen evolution reaction," *Proceedings of the National Academy of Sciences,* vol. 110, no. 49, pp. 19701-19706, 2013.

[140] D. Voiry *et al.*, "Conducting MoS_2 Nanosheets as Catalysts for Hydrogen Evolution Reaction," *Nano Letters,* vol. 13, no. 12, pp. 6222-6227, 2013, doi: 10.1021/nl403661s.

[141] N. H. Attanayake *et al.*, "Effect of Intercalated Metals on the Electrocatalytic Activity of 1T-MoS_2 for the Hydrogen Evolution Reaction," *ACS Energy Letters,* vol. 3, no. 1, pp. 7-13, 2018, doi: 10.1021/acsenergylett.7b00865.

[142] M. A. R. Anjum, H. Y. Jeong, M. H. Lee, H. S. Shin, and J. S. Lee, "Efficient Hydrogen Evolution Reaction Catalysis in Alkaline Media by All-in-One MoS_2 with Multifunctional Active Sites," *Advanced Materials,* vol. 30, no. 20, p. 1707105, 2018.

[143] P. D. Tran *et al.*, "Coordination polymer structure and revisited hydrogen evolution catalytic mechanism for amorphous molybdenum sulfide," *Nature Materials,* vol. 15, no. 6, pp. 640-646, 2016, doi: 10.1038/nmat4588.

[144] J. W. D. Ng *et al.*, "Gold-supported cerium-doped NiO_x catalysts for water oxidation," *Nature Energy,* vol. 1, no. 5, p. 16053, 2016, doi: 10.1038/nenergy.2016.53.

[145] Y.-Y. Chen *et al.*, "Self-Templated Fabrication of $MoNi_4/MoO_{3-x}$ Nanorod Arrays with Dual Active Components for Highly Efficient Hydrogen Evolution," *Advanced Materials,* vol. 29, no. 39, p. 1703311, 2017.

[146] Y. Zhou *et al.*, "Topological Formation of a Mo–Ni-Based Hollow Structure as a Highly Efficient Electrocatalyst for the Hydrogen Evolution Reaction in Alkaline Solutions," *ACS Applied Materials & Interfaces,* vol. 11, no. 24, pp. 21998-22004, 2019.

[147] V. K. Singh, U. Gupta, B. Mukherjee, S. Chattopadhyay, and S. Das, "MoS2 Nanosheets on MoNi4/MoO2 Nanorods for Hydrogen Evolution," *ACS Applied Nano Materials,* vol. 4, no. 1, pp. 886-896, 2021/01/22 2021, doi: 10.1021/acsanm.0c03296.